上部マントルにおけるペリドタイトの部分融解と玄武岩質マグマの生成について

廣瀬　敬

学位論文

Partial Melting of Peridotite in the Upper Mantle and Genesis of Basaltic Magmas

上部マントルにおけるペリドタイトの部分融解と玄武岩質マグマの生成について

平成５年１２月 博士（理学）申請

東京大学大学院理学系研究科
地質学専攻

廣瀬　敬

ABSTRACT

Partial melting of peridotite in the upper mantle is considered to be an important process for the genesis of basaltic magmas. Melt formation from mantle peridotite by two different partial melting processes, batch melting and incremental batch melting, were experimentally performed. Although the amount of water in source peridotite is quite variable, it has influence on partial melting process. Batch melting experiments, therefore, were made under both anhydrous and hydrous conditions and the effect of water was estimated. The compositions of partial melts and degrees of melting were determined over wide pressure-temperature conditions using original methods and the genesis of basaltic magmas in the upper mantle is discussed from the present experimental results.

Numerous melting experiments have been made, but the compositions of partial melts have not ever been precisely determined due to experimental difficulties. The diamond aggregate method was developed in this study where partial melts are trapped between the pore space of diamond aggregates, and their compositions can be determined by the direct microprobe analyses. Batch melting experiments under anhydrous conditions were made in a pressure range from 10 to 30 kbar at temperatures near the solidus. The compositional change with increasing melt fractions were investigated and the effect of source peridotite compositions on partial melts was also considered using two different lherzolites. SiO_2 contents in partial melts strongly depend on pressure and MgO contents are mainly controlled by temperature, and both the contents depend little on the source

composition. In contrast, Al_2O_3, FeO, CaO and incompatible elements are controlled by the source composition as well as degree of partial melting.

The presence of water can significantly influence partial melting process which increases the degree of partial melting and changes the compositions of melts. Its effect on partial melting, however, have little been estimated quantitatively. Using the crimp method, the compositions of melts formed by partial melting of hydrous peridotite at 10 kbar were successfully determined. To minimize the iron loss, Au-Pd and Ag-Pd capsules were used as the container. The melt fractions 12-15 % can be formed at 1300°C under dry conditions, at 1200°C with 0.2 wt.% H_2O in the source and at 1100°C with 0.9 wt.% H_2O in the source. At 1300°C the presence of 0.1, 0.2 and 0.5 wt.% water in source increases the melt fraction from 12.1 % under dry condition to 18.5, 21.8 and 30.2 % respectively. Melts with less than 1.7 wt.% H_2O are close in composition to anhydrous melts formed by the same degree of partial melting. On the other hand, melts with more than 6.0 wt.% H_2O formed at about 150°C below the dry solidus temperature are enriched in SiO_2 and depleted in MgO contents. The effect of water must be considered for the genesis of even tholeiitic basalts with relatively small amounts <2 wt.% of H_2O. The relatively high amounts of water in glasses from some hot spot regions along the Mid-Atlantic Ridge can be responsible for their relatively high degrees of partial melting reflecting in thick crustal thickness in these regions.

Recent studies on MORB suggested that small fractions of melts can segregate from the host peridotite and melts are formed by near fractional melting at mid-oceanic ridges. The near

fractional melting process has not ever been estimated by the high pressure experiments. The incremental batch melting process was experimentally investigated using gel starting materials under two different conditions, and the compositions and accumulated fractions of melts were determined using the diamond aggregate method. (1) The experiments with a complete withdrawal of 3.7-9.9 % incremental melts were performed at 15 kbar with increasing temperature to 1425°C. Melt fractions formed by incremental batch melting are significantly lower than those formed by batch melting; 22.8 and 36.7 % respectively at 1425°C. The compositions of accumulated incremental melts are quite similar to those of batch melts formed by the same total degrees of partial melting. (2) Melt generation by adiabatic decompression of the mantle in a pressure range from 22.5 kbar to atmospheric pressure was considered. It is notable that the rate of melt production decreases from 22.5 kbar to lower pressures and only quite small amounts of melt are produced at depths shallower than 30 km. The composition of accumulated incremental melts strongly reflects that of increments formed at pressures higher than 10 kbar and is similar to that of batch melt formed at 15 kbar. It is important to estimate the chemical isolation between melt and solid during melt migration that controls the melt formation by batch melting or by near fractional melting.

The North Fiji Basin basalts were studied for a case study to investigate magma generation at oceanic ridges. The North Fiji Basin is the largest back-arc basin among presently active basins and the spreading ridge is regionally identical to mid-oceanic ridges. The tectonic setting, however, is complex and basalts which are quite variable in composition are divided into four magma

types; type I: N-MORB like basalts, type II: E-MORB like basalts, type III: OIB like transitional alkalic basalts, and type IV: BABB like basalts. The N-S segment is considered to be a mature segment where the spreading system is generally similar to that of normal mid-oceanic ridges with a medium spreading rate in basalt chemistry and ridge topography. The relatively long distance more than 300 km from the trench and the temporal evolution within 10 million years can form seafloor spreading in back-arc basin similar to that at normal mid-oceanic ridges. In contrast, the N160 segment is considered to be in a stage of crustal extension rather than seafloor spreading, and the geochemically enriched type II and III basalts are dominant. The type IV basalts appear only in the 170E segment which is close to the trench about 150 km in distance. It suggests that the genetic influence of the supra-subduction zone mantle is restricted to the area close to the convergent margin. The type III and IV basalts have distinct major element compositions and higher H_2O contents than the type I and II basalts, showing their lower temperature origin. He isotope ratios are generally higher than the mean MORB values, suggesting that the source mantle for the North Fiji Basin basalts includes slightly primitive mantle component.

Contents

I. General introduction

Partial melting of peridotite in the upper mantle is considered to be an important process for the genesis of basaltic magmas. Numerous melting experiments have been made, but they are still insufficient from the following points of view; (1) the changes in melt compositions and degrees of melting formed by partial melting of a peridotite under varying pressure and temperature conditions have not been precisely understood, (2) most of the previous experiments were made under anhydrous conditions, and (3) the previous experiments could only be applied to melt generation by batch melting processes. The present experiments were performed on the partial melting of lherzolites for three different conditions; batch melting both under anhydrous conditions (session II) and under hydrous conditions (session III) and incremental batch melting (session IV).

One important aspect of the present study is to determine both the melt composition and degree of partial melting formed by these three different conditions. The degree of partial melting is one of the most principal data in modelling the melt generation in the upper mantle (e.g. Klein and Langmuir, 1987; Mckenzie and Bickle, 1988). However, they were poorly determined by the previous experiments and their quantitative estimation has been insufficient (e.g. Mysen and Kushiro, 1977; Jaques and Green, 1980). The melt composition and degree of partial melting are significantly changed by the presence of water and also depend on the melting process. Their effects on melt generation in the upper mantle are quantitatively estimated and discussed in this thesis.

There have been a debate on the method to determine the compositions of partial melts due to the experimental problems such as overgrowth of adjacent minerals at quenching which significantly modifies the melt compositions (e.g. Mysen and Kushiro, 1977). To overcome this quench problem, some different methods were applied to the melting experiments since 1980's. Jaques and Green (1980) nearly successfully determined the degrees of melting and the melt compositions, but their determination included the uncertainty in modal analysis and in calculation due to compositional zoning (Takahashi and Kushiro, 1983). Using the "peridotite capsule method" or "sandwich method" (e.g. Stolper, 1980; Takahashi and Kushiro, 1983; Fujii and Scarfe, 1985; Falloon et al., 1988), the compositions of melts saturated in mantle minerals were determined. The bulk compositions, however, were significantly modified by addition of basalts and the melt compositions also depend on those of added basalts. Moreover, the degrees of melting cannot be determined by their method. With the "diamond aggregate method" and "crimp method" presented here, both the compositions and fractions of melts formed by partial melting from the peridotites are successfully determined without these problems, and the compositional change with increasing degree of partial melting can be described over a wide pressure range (session II) (e.g. Kushiro and Hirose, 1992; Johnson and Kushiro, 1992; Hirose and Kushiro, 1992 and 1993; Baker et al., 1992; Baker and Stolper, 1993).

The presence of H_2O probably plays an important role on the partial melting process for most basaltic magmas. Most of the previous melting experiments, however, were made under anhydrous conditions, and the effect of H_2O on partial melt

composition and degree of partial melting has little been estimated quantitatively (Mysen and Kushiro, 1977; Green, 1973; Kushiro, 1990). The melting experiments in both Fe- and H_2O-bearing systems include another experimental problem that iron contents are modified by reaction with the containers. Two improvements were achieved in the present study compared to Kushiro (1990), in which the compositions of melts formed by hydrous partial melting of lherzolite were determined using Fe-presaturated Pt capsules and the sandwich method. To minimize the Fe loss, the Au-Pd capsules were used as the containers in the present hydrous experiments (Kawamoto and Hirose, 1993) (session III), and the compositions and fractions of partial melts with relatively small amounts of H_2O (0.5 wt.%~) could be determined. The abundances of H_2O in basalt are quite variable ranging from 0.2 to 2.0 wt.% for the tholeiitic basalt magmas (e.g. Muenow et al., 1990), and the influence of the presence of water must be taken into account for the genesis of basaltic magmas with relatively high water contents.

In session IV, the melt formation by non-modal incremental batch melting process was experimentally investigated with the diamond aggregate method. It is recently suggested that the melt generation are controlled by near fractional melting process (e.g. Mckenzie, 1985; Johnson et al.,1990; Iwamori, 1993). Near fractional melting processes, however, have not been sufficiently understood partly due to the lack of incremental batch or fractional melting experiments. Kinzler and Grove (1992a,b) attempted calculations to integrate the compositions of melts formed by near fractional melting, but the degrees of partial melting cannot be predicted by their integrations. The incremental batch melting with complete melt withdrawal was made (1) at 15 kbar with

increasing temperature and (2) considering the melt formation from adiabatically upwelling mantle by decompression from 22.5 kbar to atmospheric pressure. Both the compositions and the volume of incremental melts were determined here. The melt formation by the incremental batch partial melting of lherzolite is discussed in comparison with that by the batch melting process.

In session V, the petrology of the North Fiji Basin is discussed as the case study of ridge magmatism. It is the oldest and largest active back-arc basin situated in the southwestern Pacific. The widely ranged chemical compositions of the collected glasses reflecting the complex tectonic settings are described, and their petrogenesis and the evolution of the back-arc basin magmatism are discussed.

II. Partial Melting of Peridotite at High Pressures; Batch Melting under Anhydrous Conditions

ABSTRACT

The compositions of melts formed by partial melting of two relatively fertile spinel lherzolites were determined at pressures between 10 and 30 kbar under dry conditions using a layer of diamond aggregates sandwiched between peridotite layers. Partial melts segregate and migrate into the pore space between diamond grains soon after their formation. Overgrowth of minerals at quenching modifies the composition of coexisting melt, but this modification does not extend to the trapped melt in the diamond layer. Microprobe analyses of the trapped melt, therefore, can determine the melt compositions without the quench problem. Melts formed by low degrees of partial melting (~5%) can be analyzed successfully by this method. The effect of the source composition on partial melting was examined between the two different lherzolites. The change in oxide compositions with increasing temperature is presented in a wide pressure range. Both partial melts have nearly the same SiO_2 and MgO contents at the same pressure and temperature conditions regardless of their different Mg/(Mg+Fe) ratios, suggesting that SiO_2 and MgO contents in partial melts depend little on the source composition. In contrast, FeO, Al_2O_3, CaO and incompatible elements are controlled by the composition of the source peridotite as well as by the degree of partial melting. In the normative projections, the differences of

the lherzolite compositions do not significantly shift the isobaric compositional trends of the partial melts.

II-1. Introduction

Partial melting of peridotites in the upper mantle is believed to be an important process to understand the origin of basaltic magmas. Numerous high pressure experimental studies have been attempted to determine the compositions of such partial melts in both synthetic and natural peridotite systems. Yet, there are still problems concerning the method of determination of the compositions of quenched liquid. Melting experiments with peridotite capsules and those by the sandwich method were fairly successful in the determination of major elements in equilibrium melts (Stolper, 1980; Takahashi and Kushiro, 1983; Fujii and Scarfe, 1985; Falloon et al., 1988). However, the compositions of melts determined by these methods, particularly the abundances of incompatible elements, are affected and modified by the materials added to the host peridotites and, therefore, they do not represent the true partial melt compositions. Such modification is especially large when the degree of partial melting is low. In the present experiments, analyzable amounts of partial melts can be extracted from the host peridotites at high pressures by a new method using aggregates of diamond grains which provide pore space for melt extraction (e.g. Kushiro and Hirose, 1992; Johnson and Kushiro, 1992; Hirose and Kushiro, 1993; Kushiro, 1993; Baker and Stolper, 1993) (Fig. 1b). It is anticipated that microprobe analyses of these separated melts would give the true partial melt compositions.

Melts formed by low degrees of partial melting (as low as 5%) can also be extracted and determined successfully. Recent studies suggest that small melt fractions can segregate from the host peridotite (e.g. Mckenzie, 1985; Johnson et al., 1990; Riley and Kohlstedt, 1991). Determination of the compositions of equilibrium partial melts formed by low degrees of partial melting would contribute to modelling magma generation by such fractional melting.

The source materials for basalt magmas (upper mantle peridotite) would be heterogeneous and so the effect of different source compositions on partial melts should be investigated. In this paper, we present the new experimental results on anhydrous melting of two different relatively fertile spinel lherzolites which are different in Mg/(Mg+Fe) ratio and Cr/(Cr+Al) ratio in spinel. One is a spinel lherzolite from Salt Lake Crater, Hawaii (HK66101703, designated HK-66 hereafter) (Takahashi and Kushiro, 1983; Kushiro, 1968). The other one designated KLB-1 is a less fertile spinel lherzolite from Kilborne Hole crater in New Mexico (Takahashi, 1986). The compositions of partial melts formed near the solidi of these two spinel lherzolites have been determined using the present new method, and the effects of pressure, temperature and composition of the source peridotite on the composition of partial melts are discussed.

II-2. Experimental and analytical method

In the present experiments, partial melts separated from the host peridotite into pore space between diamond grains at high

pressures (Fig. 1b). Three different configurations of charges were tested to obtain equilibrium partial melts (Kushiro and Hirose, 1992): (i) an aggregate of diamond powder (40-60 μm in diameter) is packed on top of tightly packed peridotite powder (the ratio of diamond to peridotite is 1:1-1:2), (ii) a thin layer (< 0.5 mm thick) of diamond powder is sandwiched between peridotite powder (5-50 μm), (iii) a chip of loosely sintered diamond powder is embedded in peridotite powder (Fig. 1a). The sintered diamond was made by heating diamond powder at 10 kbar and 1300°C for 1 hour prior to the experiments. In all the configurations, pore space between diamond grains was preserved at pressures at least to 30 kbar before the run. Although partial melts separate and migrate into the pore space between diamond grains soon after their formation, chemical contact would be maintained with melts in the peridotite layers. Even in a 1 hour run, melt already filled the pore space between diamond grains. As shown below, equilibrium partial melts can be obtained with configurations (ii) and (iii).

The starting materials were two natural peridotites. The charges were loaded in graphite capsules 2 mm in diameter and 3.5 mm in length. To ensure dry conditions, the graphite capsules loaded with peridotite and diamond were preheated at about 1000°C before sealing in Pt capsules. The runs were made in a temperature range from 1250° to 1525°C and in a pressure range from 10 to 30 kbar with a piston-cylinder type apparatus. Calibration for pressure and other experimental procedures with this apparatus have been described elsewhere (Kushiro, 1976). Temperature was measured and controlled by $Pt/Pt_{90}Rh_{10}$ thermocouples. After quenching the charges were sectioned longitudinally and polished for microprobe analyses. It is easy to

polish because the surface of the diamond grains changes into graphite during the run. Analyses were made with a scanning electron microscope (JEOL JSM-840) with Link EDS systems. The quenched melts trapped between diamond grains were 10-50 μm in size in most cases. Analytical conditions were 15 KV accelerating voltage, 1 nA specimen current and 60-80 seconds counting time.

II-3. Attainment of equilibrium

It is important to check whether or not chemical equilibrium is attained between the melts segregated into the pore space in the diamond layer and the residual phases of the peridotite. In the preceding study (Kushiro and Hirose, 1992), we conducted experiments on the synthetic system Mg_2SiO_4-$NaAlSiO_4$-SiO_2 of which phase relations (liquidus boundary between forsterite and enstatite solid solution) had been determined at high pressures (Kushiro, 1968). The results indicated that equilibrium melts can be obtained with configurations (ii) and (iii) within 24 hours at least at 10, 15 and 20 kbar. However, with configuration (i) unexpectedly low-pressure melt was formed. It is probably due to the fact that the pore space in the diamond layer was too large to be filled with melt, resulting in the melt pressure to be lower than the load pressure. It is important, therefore, that the volume of pore space in the diamond layer should be reduced to less than that of equilibrium melt. We used sintered diamond chips of which the pore space is about 50 volume% as estimated from the SEM images. In most of runs the sintered diamond chips occupy less than 3% in volume of peridotite powder, so that only 1.5% partial melt can fill

up the pore space. The pore space was reduced to less than 1% by using a smaller sintered diamond chip when the degrees of melting were very low. In the present experiments, configuration (iii) which contains a chip of loosely sintered diamond grains was used in most of the runs and configuration (ii) was also used for a few runs.

The duration necessary to obtain equilibrium melts was also examined in the same synthetic system and with spinel lherzolite KLB-1. The results from the synthetic system indicated that at least 24 hours are necessary to obtain equilibrium melts at 15 kbar and 1400°C (Kushiro and Hirose, 1992). In the present experiments, the time-dependent compositional changes of melts have been examined for KLB-1 with configuration (iii). The results at 15 kbar and 1350°C for three different run durations 6, 24 and 67 hours are shown in Table 1. In the 6 hour run, the Al_2O_3 content is relatively high and the MgO content is relatively low. After 24 hours, the abundances of major elements reach nearly constant values. Compositional zoning in respect of Mg/(Mg+Fe) ratio in minerals is hardly observed in both 24 and 67 hour runs. On the other hand, weak compositional zoning is observed for Al_2O_3 and CaO in pyroxenes even in the 24 hour run, but is minimal in the 67 hour run. From this point of view, completely equilibrium melts cannot be obtained in 24 hours and the bulk equilibrium is nearly achieved after 67 hours. However, the composition of the partial melt changes very little after 24 hours. This means that the effect of relic pyroxenes on the composition of melts is very small after 24 hours. The melt formed at 10 kbar and 1250°C for 56 hours (run #1) is close in composition to a cotectic melt at 10 kbar and 1260°C obtained by Kinzler and Grove (1992a).

The Fe/Mg partitioning between olivine and liquid observed in the present experiments is in good agreement with that in the previous work (e.g. Takahashi and Kushiro, 1983) (Table 4). As shown in the preceding experiments (Johnson and Kushiro, 1992; Kushiro and Hirose, 1992), Mg^{2+} and Fe^{2+} in melts reach constant values within shorter run durations than ions with smaller diffusivities such as Si^{4+} and Al^{3+}. The Fe/Mg ratio, therefore, cannot be used for judging perfect equilibration of partial melting.

II-4. Starting materials of natural peridotite

Melting experiments were conducted on two different natural spinel lherzolites, HK-66 and KLB-1. Both have relatively fertile compositions, being enriched in Al_2O_3 and CaO and depleted in MgO and Cr_2O_3 compared with the world average composition for spinel lherzolite xenoliths by Maaløe and Aoki (1977) (Table 2). The differences between the two lherzolites are observed in the modal amount of orthopyroxene, Mg/(Mg+Fe) ratio, Cr/(Cr+Al) ratio of spinel, and abundances of incompatible elements. Lherzolite HK-66 consists of 27% olivine, 57% orthopyroxene, 14% clinopyroxene and 2% spinel by weight, whereas KLB-1 consists of 58% olivine, 25% orthopyroxene, 15% clinopyroxene and 2% spinel. The Fo contents in olivine are 85.0, and 89.1 (mol %) for HK-66 and KLB-1, respectively. Takahashi and Kushiro (1983) determined the solidus of HK-66 and attempted to determine the equilibrium melt compositions near the solidus by the sandwich method. The melting behavior of lherzolite KLB-1 was originally studied by Takahashi (1986), and the degrees of partial melting and the

compositions of partial melts were estimated by Takahashi et al. (1992) over a pressure range from 1 bar to 65 kbar.

II-5. Experimental results

Melting experiments were made at temperatures just above the solidi of HK-66 and KLB-1 under dry conditions (Fig. 2). Details of the run conditions and the residual assemblages are summarized in Table 3. In some cases, partial melts were detected at temperatures slightly below the solidus reported by Takahashi (1986). The compositions of partial melts (estimated degree of partial melting 5~40%) determined with the present method are shown in Table 4. The solidus temperature of KLB-1 was reported to be about 50°C higher than that of HK-66 above 10 kbar. The degree of melting of HK-66, therefore, is always higher than that of KLB-1 under the same pressure and temperature conditions. The calculated degree of melting (F) is listed in Table 4. It was approximately estimated from Na_2O contents in melts. These estimations, however, would give maximum values, because of the presence of small amounts of Na in clinopyroxene and plagioclase.

Homogeneity of melts distributed in the diamond layer was examined in the preceding experiments (Kushiro and Hirose, 1992) by analyzing many different quenched melts within the diamond layer. The ranges for major oxide components are small (Table 1). The quench minerals were scarcely observed in the melt pools in the diamond layer.

At 10 kbar, the composition of melts formed by partial melting of KLB-1 just above the solidus is nepheline normative and

alkali-olivine basaltic, whereas that of HK-66 is olivine tholeiitic and within the compositional range of high alumina basalt (Al_2O_3 >18%) (Kuno, 1960). At higher temperatures melts are also olivine tholeiitic, but they become depleted in albite component and enriched in hypersthene component. Above 15 kbar, melts formed near the solidi are alkali basaltic or alkali picritic. A melt with nephelinite composition (norm nepheline >10%) was formed from HK-66 at 15 kbar. With increasing pressure, SiO_2 contents decrease form about 50 wt% at 10 kbar to about 46 wt% at 30 kbar. MgO and FeO contents are higher at higher pressures, and melts formed near the solidi are picritic at 30 kbar.

5.1. Systematic changes in major elements in melts under varying pressure and temperature conditions

SiO_2 contents in partial melts are strongly dependent on pressure (Fig. 3); they decrease with increasing pressure from 50-52 wt% at 10 kbar to 45-47 wt% at 30 kbar. At a given pressure, SiO_2 contents are nearly constant regardless of the degree of partial melting in the present pressure-temperature range. They differ little (≤1wt%) between melts of HK-66 and KLB-1 under the same pressure and temperature conditions, despite the SiO_2 contents of these lherzolites being significantly different. On the other hand, MgO contents in melts are dependent on temperature, but are relatively insensitive to pressure (Fig. 4); at a given pressure, they increase by 1 wt% with increase in temperature of about 20°C. MgO values are similar in the partial melts of the two peridotites at the same temperatures despite significantly different Mg/(Mg+Fe) ratios.

FeO contents in melts of HK-66 and KLB-1 appear to depend on pressure (Fig. 5a) and in contrast to MgO they are considerably different in the two lherzolites. At a given pressure FeO contents in melts increase with increasing degree of partial melting at pressures below 20 kbar, but above 25 kbar they are nearly constant or decrease though there are no data for low degrees of partial melting (<10%) above 25 kbar (Fig. 5b). Al_2O_3 contents in melts decrease with increasing degree of partial melting (Fig. 6a). The Al_2O_3 contents in melts of HK-66 are higher than those of KLB-1 at the same degree of partial melting and thus reflect the bulk Al_2O_3 contents in source lherzolites. Fujii and Scarfe (1985) showed that Cr/(Cr+Al) ratio of spinel correlates well with Al_2O_3 in melts. The Cr/(Cr+Al) ratio of spinel in HK-66 is lower than that in KLB-1, being consistent with their observation. With increasing pressure, Al_2O_3 contents in melts decrease at the same degree of partial melting that is well observed in HK-66 which is enriched in orthopyroxene. The behavior of CaO in melts is complex; with increasing temperature, it increases initially probably due to depletion or elimination of spinel and then decreases after clinopyroxene disappears (Fig. 6b). The CaO contents in melts are thus strongly dependent on the composition of the source spinel lherzolites.

5.2. Comparison with sandwich method

Determination of the equilibrium melt compositions by the sandwich method has the problems caused by addition of basalt to peridotite as follows;

(i) The bulk composition is changed. Enrichment in the basaltic component modifies the equilibrium melt composition especially when the degree of melting is low. The effect of changing bulk composition on partial melt composition is significant for Al_2O_3, CaO and incompatible elements as shown in the previous paragraph. For example, at 20 kbar and 1375°C (run #8) the abundances of these elements determined by the sandwich method (Takahashi and Kushiro, 1983) are significantly different from those obtained by the present method; the K_2O content is 0.25 wt% in our results compared to 1.0 wt% by the sandwich method (Table 5). In the latter experiments, alkali basalt with K_2O 1.7 wt% was sandwiched. CaO contents in melts determined by the sandwich method (Takahashi and Kushiro, 1983) were also considerably affected by the added basalts.

(ii) It would be possible that the sandwiched melt is not homogenized with partial melts formed apart from the sandwiched layer. Until they are homogenized, melt in the sandwiched layer would be in only local equilibrium with the surrounding peridotite. It should be also emphasized that the local bulk composition could be remarkably different from the original peridotite composition. Homogenization scale of SiO_2 in melt is about 0.3mm in 24 hours using interdiffusion coefficient $D \approx 10^{-8}$ cm^2/s at 1300°C (Koyaguchi, 1989), which is much shorter than the capsule. The elements of low diffusivities in melts such as SiO_2 and Al_2O_3 could be thus modified (Fig. 7).

Falloon and Green (1987) made the sandwich experiments using the basalts of compositions which were expected to be close to those of the partial melts formed from the adjacent peridotite at each pressure and temperature condition to minimize the effect of

the bulk compositional change. Their results are consistent with the present study, suggesting that equilibrium melt composition is not modified significantly if added basalt is carefully chosen.

5.3. Compositional trends of melts during isobaric partial melting of lherzolites

The compositions of partial melts determined in this study are plotted on a ternary projection ol-ne-Q of the basalt tetrahedron (Fig. 8) and on Walker's ternary projections ol-pl-Q and ol-di-Q (Fig. 9). Isobaric compositional trends are recognized as single lines in these projections. As shown in Figs. 8 and 9, the melt composition moves toward the hypersthene apex with increasing temperature at constant pressure. It is also clear that the isobaric trends shift toward the olivine apex with increasing pressure. Melts become progressively poorer in normative quartz as pressure increases to 30 kbar. The present results are in good agreement with those by Takahashi and Kushiro (1983) in these respects.

The compositions of melts formed in both HK-66 and KLB-1 approximately lie along the same isobaric line at the same pressure. This result means that the above-mentioned compositional differences between the two different lherzolites do not significantly affect the isobaric trends in the normative projections.

In Walker's ternary projection ol-di-Q, the present results do not show a marked pressure dependence of diopside component as reported by Takahashi and Kushiro (1983) (Fig. 9b). The pressure dependence of olivine component should be observed in this projection at higher degrees of partial melting after clinopyroxene disappears.

II-6. Discussion

It is very important to evaluate the effects of the source peridotite compositions on the partial melt compositions. In the sandwich experiments, the compositions of pooled melts seem to form a "univariant curve" on the ternary projections (Figs. 9a and b), although the bulk compositions are quite variable due to the addition of basalts powder (Takahashi and Kushiro; 1983; Fujii and Scarfe, 1985; Falloon et al., 1988). And this curve determined in this study is nearly identical for HK-66 and KLB-1, and is also close to that determined by Takahashi and Kushiro (1983). It suggests that this univariant curve where liquids are saturated olivine and orthopyroxene and/or clinopyroxene is little dependent on the bulk compositions.

The present experiments show the following behavior of major elements in melts formed by partial melting of the two relatively fertile spinel lherzolites. (1) SiO_2 and MgO contents depend little on the compositions of the source lherzolites (Figs. 3 and 4). (2) SiO_2 contents depend little on the degree of partial melting, but strongly depend on pressure. (3) MgO contents are controlled mainly by temperature. (4) In contrast, the abundances of FeO, Al_2O_3, CaO and incompatible elements are significantly affected by the degree of partial melting and by the compositions of source peridotites. Fujii and Scarfe (1985) already made these observations by changing bulk compositions at 10 kbar in their experiments. It should be noted that FeO content in melts could be used as a depth indicator if Mg/(Mg+Fe) ratio in the source peridotite is known (Klein and Langmuir, 1987). These results imply that when the composition of primary magma is known, the

pressure and temperature conditions of its generation from a fertile lherzolite can be approximately estimated from SiO_2 and MgO contents.

Theoretical, experimental and geochemical studies (e.g. Mckenzie, 1985; Johnson et al., 1990; Riley and Kohlstedt, 1991) suggest that melt can segregate from host peridotite even when melt fraction is very small. And the models of fractional melting have recently been applied to magma genesis at mid-oceanic ridges (e.g. Klein and Langmuir, 1987; Mckenzie and Bickle, 1988). Yet, some magnesian MORBs have similar compositions to melts formed by batch partial melting at about 10 kbar as shown in some melting experiments (e.g. Kushiro, 1972; Fujii and Bougault, 1983; Fujii and Scarfe, 1985). The present results also indicate that the partial melt formed at 10 kbar (run #2) is close in composition to one of the magnesian MORB, 519-4-2 from FAMOUS area (Table 6) (Bryan and Moore, 1977). The sandwich experiments showed that compatible major elements of added basalts reach equilibrium with surrounding peridotite within 24 hours (e.g. Takahashi and Kushiro, 1983; Fujii and Scarfe, 1985). As the grain size in the mantle would be much larger than that used in the experiments, the time for equilibration in these experiments cannot be applied directly. However, the time for equilibration should also depend on the flow rate of melt in the mantle. The time for melts to ascend through mantle peridotite must be much longer than 24 hours. It suggests that during their ascent through the mantle peridotite, compatible elements could interact between the melts and peridotites and reequilibrate at shallower depths (Falloon et al., 1988). The compositions of ascending melts, therefore, would become close to

those of melts formed by batch partial melting at such shallow depths of about 10 kbar.

TABLE 1. Results of runs with different run durations on KLB-1 at 15 kbar and 1350°C

	6 hrs	24 hrs	67 hrs
SiO2	49.53	49.13 (48.82-49.48)†	49.44
TiO2	0.51	0.60 (0.43-0.69)	0.55
Al2O3	16.28	15.18 (14.94-15.32)	15.20
FeO*	7.54	7.54 (7.08-7.78)	7.53
MnO	0.15	0.14 (0.05-0.31)	0.11
MgO	12.45	13.11 (12.72-13.57)	13.41
CaO	11.67	12.28 (11.96-12.89)	12.00
Na2O	1.67	1.58 (1.36-1.70)	1.51
K2O	0.07	0.08 (0.06-0.15)	0.04
Cr2O3	0.13	0.36 (0.24-0.47)	0.21
Total	100.00	100.00	100.00
Fo mol %	90.7	90.6	90.6
Kd (Fe/Mg)	0.302	0.321	0.331

*: all Fe as FeO

†: the range of analyses of the trapped melt pools

TABLE 2. Compositions of spinel lherzolites KLB-1 and HK-66 and their constituent minerals

	KLB-1	HK-66	Spinel Lherzolite Xenoliths†
SiO2	44.48	48.02	44.20
TiO2	0.16	0.22	0.13
Al2O3	3.59	4.88	2.05
FeO*	8.10	9.90	8.29
MnO	0.12	0.14	0.13
MgO	39.22	32.35	42.21
CaO	3.44	2.97	1.92
Na2O	0.30	0.66	0.27
K2O	0.02	0.07	0.06
P2O5	0.03	0.07	0.03
Cr2O3	0.31	0.25	0.44
NiO	0.25	n.d.	0.28
Total	100.02	99.53	100.01

KLB-1††	ol	opx	cpx	sp
SiO2	39.64	54.24	51.13	0.06
TiO2	0.00	0.11	0.58	0.11
Al2O3	0.03	4.97	7.40	58.48
FeO*	10.52	6.57	3.11	10.68
MnO	0.16	0.16	0.10	n.d.
MgO	48.25	32.16	14.70	21.61
CaO	0.08	0.85	19.54	0.00
Na2O	0.01	0.12	1.72	0.00
K2O	0.00	0.00	0.01	0.00
Cr2O3	0.01	0.34	0.78	7.82
NiO	0.39	0.11	0.11	0.43
Total	99.09	99.63	99.18	99.19
Mg/(Mg+Fe)	0.891	0.897	0.894	0.783

HK-66†††	ol	opx	cpx	sp
SiO2	38.76	53.50	50.93	0.12
TiO2	0.00	0.11	0.55	0.21
Al2O3	0.00	5.27	7.35	61.31
FeO*	14.41	8.71	4.30	15.34
MnO	0.17	0.13	0.09	0.13
MgO	45.89	31.13	14.62	19.53
CaO	0.07	0.71	18.75	0.04
Na2O	0.00	0.13	1.96	0.00
Cr2O3	0.00	0.16	0.50	2.66
NiO	0.35	n.d.	n.d.	0.45
Total	99.65	99.85	99.05	99.79
Mg/(Mg+Fe)	0.850	0.864	0.858	0.694

†: Average of 384 spinel lherzolites (Maaløe and Aoki, 1977)
††: data from (Takahashi, 1986)
†††: data from (Takahashi and Kushiro, 1983)

TABLE 3. Details of runs

HK-66

Run #	P (kbar)	T (°C)	Duration (hr)	Residue	Configuration
1	10	1250	56	ol, opx, cpx, sp, pl	(iii)
2	10	1300	24	ol, opx, cpx	(ii)
3	10	1350	24	ol, opx	(ii)
4	15	1275	24	ol, opx, cpx, sp	(ii)
5	15	1350	23	ol, opx	(iii)
6	15	1400	24	ol, opx	(ii)
7	20	1350	24	ol, opx, cpx, sp	(iii)
8	20	1375	24	ol, opx, cpx	(iii)
9	20	1425	24	ol, opx	(iii)
10	25	1425	24	ol, opx, cpx	(iii)
11	25	1450	24	ol, opx	(iii)
12	30	1475	12	ol, opx	(iii)
13	30	1500	12	ol, opx	(iii)

KLB-1

Run #	P (kbar)	T (°C)	Duration (hr)	Residue	Configuration
14	10	1250	56	ol, opx, cpx, sp, pl	(iii)
15	10	1300	24	ol, opx, cpx, sp	(ii)
16	10	1350	24	ol, opx	(ii)
17	10	1400	24	ol, opx	(ii)
18	15	1300	24	ol, opx, cpx, sp	(iii)
19	15	1350	24	ol, opx, cpx	(ii)
20	15	1400	44	ol, opx	(iii)
21	20	1375	24	ol, opx, cpx	(iii)
22	20	1425	24	ol, opx, cpx	(iii)
23	25	1425	24	ol, opx, cpx	(iii)
24	25	1450	24	ol, opx, cpx	(iii)
25	30	1500	12	ol, opx, cpx	(iii)
26	30	1525	12	ol, opx, cpx	(iii)

TABLE 4. Compositions of the partial melts

HK-66						
Run	1	2	3	4	5	6
P (kbar)	10	10	10	15	15	15
T (°C)	1250	1300	1350	1275	1350	1400
SiO2	50.83	49.60	50.37	49.83	48.42	48.48
TiO2	1.12	0.79	0.54	1.07	0.85	0.78
Al2O3	18.57	16.49	14.53	18.80	16.60	13.06
FeO*	7.98	8.89	9.44	8.03	9.42	10.79
MnO	0.28	0.12	0.16	0.08	0.11	0.21
MgO	7.77	10.35	13.46	8.26	11.25	14.26
CaO	9.44	11.27	9.55	7.93	10.69	10.50
Na2O	3.69	2.15	1.60	5.41	2.36	1.66
K2O	0.32	0.15	0.14	0.59	0.09	0.10
Cr2O3	n.d.	0.19	0.21	n.d.	0.21	0.16
Total	100.00	100.00	100.00	100.00	100.00	100.00
CIPW Norm						
os	2.13	0.89	0.83	3.49	0.53	0.59
ab	20.60	18.22	13.57	27.26	20.01	14.04
an	32.07	34.98	32.11	25.28	34.52	27.94
ne	3.09			10.02		
di	19.59	17.11	12.41	11.46	15.10	19.65
hy		12.71	28.76		5.23	13.34
ol	21.01	14.59	11.29	20.47	22.98	22.95
il	1.52	1.50	1.03	2.03	1.62	1.48
Fo mole %	85.6	87.1	87.7	85.9	87.0	87.4
Kd (Fe/Mg)	0.292	0.307	0.356	0.301	0.318	0.339
F†	0.179	0.307	0.412	0.122	0.279	0.398

HK-66							
Run	7	8	9	10	11	12	13
P (kbar)	20	20	20	25	25	30	30
T (°C)	1350	1375	1425	1425	1450	1475	1500
SiO2	47.41	47.55	47.12	46.82	47.41	45.89	45.59
TiO2	1.44	1.18	1.17	1.16	0.82	1.40	1.18
Al2O3	15.92	15.61	13.96	13.81	12.29	12.43	12.35
FeO*	10.38	10.58	10.47	11.68	11.69	12.91	12.56
MnO	0.29	0.14	0.12	0.21	0.12	0.20	0.30
MgO	10.85	12.01	14.74	13.28	15.54	14.30	15.98
CaO	9.26	9.96	10.23	10.22	10.17	9.89	9.67
Na2O	3.91	2.61	1.90	2.34	1.58	2.51	2.02
K2O	0.42	0.25	0.21	0.34	0.19	0.35	0.18
Cr2O3	0.12	0.11	0.08	0.14	0.19	0.12	0.17
Total	100.00	100.00	100.00	100.00	100.00	100.00	100.00
CIPW Norm							
os	2.49	1.48	1.24	2.01	1.13	2.07	1.07
ab	19.02	20.31	16.09	15.94	13.40	12.85	13.15
an	24.70	30.21	28.98	26.22	25.93	21.68	24.17
ne	7.61	0.95		2.10		4.52	2.11
di	17.35	15.67	17.64	19.99	19.95	22.33	19.39
hy			2.60		7.82		
ol	26.10	29.15	31.23	31.52	30.23	33.89	37.88
il	2.74	2.24	2.22	2.21	1.54	2.66	2.23
Fo mole %	85.7	86.2	86.7	86.5	87.9	86.5	87.2
Kd (Fe/Mg)	0.311	0.324	0.385	0.316	0.326	0.308	0.333
F†	0.169	0.253	0.347	0.282	0.418	0.263	0.327

†, degree of partial melting calculated from Na2O abundance

TABLE 4. continued

KLB-1							
Run	14	15	16	17	18	19	20
P (kbar)	10	10	10	10	15	15	15
T (°C)	1250	1300	1350	1400	1300	1350	1400
SiO2	51.32	50.49	50.67	51.59	50.71	49.13	49.88
TiO2	1.09	0.65	0.42	0.44	1.04	0.60	0.45
Al2O3	19.09	17.94	14.61	12.58	19.31	15.18	13.78
FeO*	6.38	6.69	7.64	7.95	6.37	7.54	7.92
MnO	0.23	0.11	0.13	0.29	0.14	0.14	0.13
MgO	8.14	10.08	13.39	16.41	8.31	13.11	15.74
CaO	8.85	11.37	11.17	9.42	7.75	12.28	10.69
Na2O	4.60	2.47	1.50	0.91	5.47	1.58	1.04
K2O	0.27	0.09	0.19	0.05	0.73	0.08	0.04
Cr2O3	0.03	0.11	0.28	0.36	0.17	0.36	0.33
Total	100.00	100.00	100.00	100.00	100.00	100.00	100.00
CIPW Norm							
os	1.54	0.36	1.13	0.30	4.33	0.47	0.24
ab	33.78	19.68	12.72	7.70	29.61	13.45	8.80
an	30.69	38.45	32.66	30.21	26.04	34.19	32.93
ne	2.79				9.07		
di	10.70	14.63	18.43	13.37	10.06	21.67	16.25
hy		15.41	24.12	43.84		12.45	28.92
ol	18.42	10.23	10.13	3.75	18.93	16.63	12.01
il	2.08	1.24	0.80	0.84	1.96	1.14	0.85
Fo mole %	89.2	89.9	91.0	93.1	89.5	90.6	91.5
Kd (Fe/Mg)	0.275	0.302	0.309	0.273	0.273	0.321	0.329
F†	0.065	0.121	0.200	0.331	0.055	0.189	0.289

KLB-1						
Run	21	22	23	24	25	26
P (kbar)	20	20	25	25	30	30
T (°C)	1375	1425	1425	1450	1500	1525
SiO2	47.47	48.74	47.97	48.37	45.67	46.77
TiO2	0.75	0.51	0.83	0.69	0.99	0.55
Al2O3	15.53	13.16	14.88	13.80	14.33	12.87
FeO*	8.51	8.80	9.43	8.47	9.59	9.81
MnO	0.18	0.24	0.00	0.07	0.17	0.29
MgO	13.94	15.69	13.36	15.88	16.73	17.82
CaO	11.11	11.06	10.23	10.93	10.64	10.63
Na2O	2.22	1.37	2.37	1.46	1.80	0.87
K2O	0.08	0.13	0.82	0.15	0.07	0.09
Cr2O3	0.21	0.30	0.11	0.18	0.21	0.30
Total	100.00	100.00	100.00	100.00	100.00	100.00
CIPW Norm						
os	0.47	0.77	4.85	0.89	0.42	0.53
ab	17.14	11.62	15.87	12.38	11.18	7.38
an	32.25	29.46	27.57	30.72	30.85	31.05
ne	0.89		2.28		2.22	
di	18.49	20.57	18.77	18.91	17.72	17.58
hy		14.64		11.85		13.17
ol	29.33	21.97	29.09	23.94	35.72	29.25
il	1.42	0.97	1.58	1.31	1.89	1.05
Fo mole %	90.2	90.8	90.5	91.2	90.1	90.8
Kd (Fe/Mg)	0.317	0.322	0.265	0.323	0.341	0.328
F†	0.135	0.219	0.126	0.206	0.166	0.347

TABLE 5. Comparison of a melt composition obtained by the present experiments at 20kbar and 1375°C with that obtained by the sandwich method (Takahashi and Kushiro, 1983)

	sandwich method	This work
SiO2	47.80	47.55
TiO2	1.55	1.18
Al2O3	15.60	15.63
FeO*	9.91	10.59
MnO	0.19	0.19
MgO	11.20	12.02
CaO	9.71	9.98
Na2O	3.33	2.61
K2O	1.00	0.25
Total	100.29	100.00

TABLE 6. Compositions of a magnesian MORB 519-4-2 (Bryan amd Moore, 1977) and a partial melt formed at 10 kbar

	519-4-2	partial melt (run #2)
SiO2	49.38	49.59
TiO2	0.74	0.79
Al2O3	16.32	16.49
FeO*	8.99	8.89
MnO	0.16	0.12
MgO	10.44	10.35
CaO	11.69	11.27
Na2O	2.17	2.15
K2O	0.07	0.15
Cr2O3	0.04	0.19
Total	100.00	100.00

a.

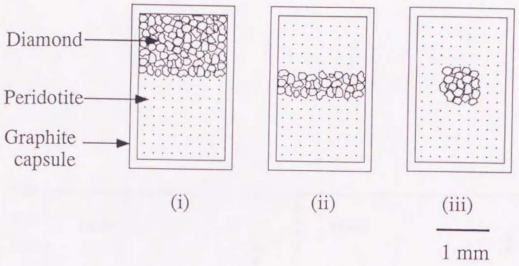

b.

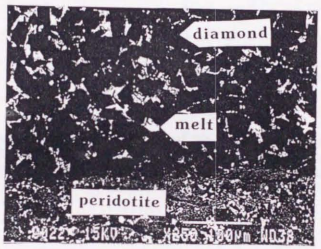

Fig. 1. (a) Three different configurations of charges used in the present experiments described in (Johnson and Kushiro, 1992; Kushiro and Hirose, 1992). Melts in equilibrium with the host peridotite can be obtained with configurations (ii) and (iii). (b) Backscattered electron image of a charge obtained at 15 kbar and 1400°C. It shows that melts are segregated and trapped between the diamond grains.

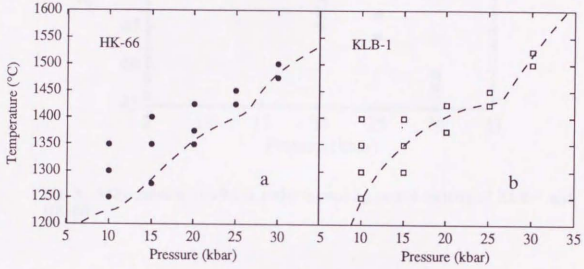

Fig. 2. Pressure-temperature conditions of the present experiments. Solidi of HK-66 and KLB-1 are from previous studies (Takahashi and Kushiro, 1983; Takahashi, 1986). In some cases, melts were detected below the reported solidus temperature.

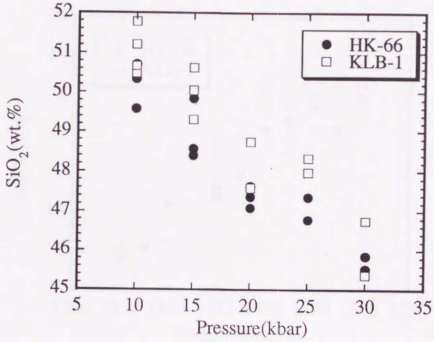

Fig. 3. SiO_2 contents (wt.%) in melts formed by partial melting of KLB-1 and HK-66.

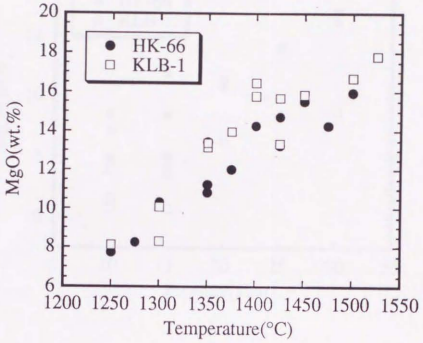

Fig. 4. MgO contents (wt.%) in melts from the two different lherzolites.

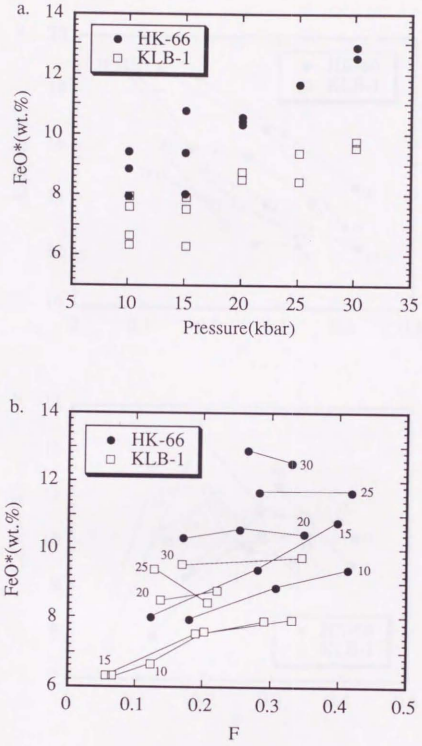

Fig. 5. FeO* contents (wt.%) in melts from KLB-1 and HK-66. F (estimated degree of partial melting) is calculated from Na_2O abundances in melt and host peridotite. The numbers indicate pressures.

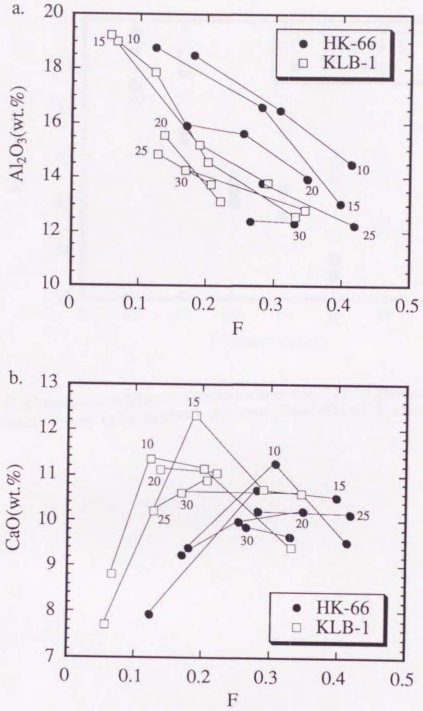

Fig. 6. (a) Al_2O_3 contents (wt.%) versus F (degree of partial melting) for melts from the two lherzolites. (b) CaO contents (wt.%) versus F (degree of partial melting) for melts from the two lherzolites.

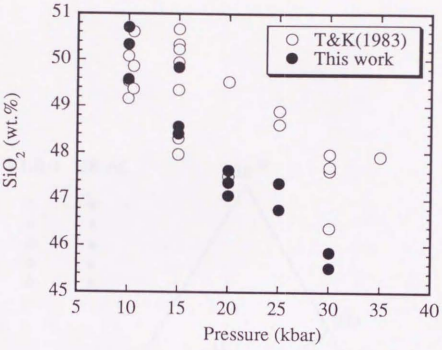

Fig. 7. Comparison of SiO_2 contents in melts obtained by the present experiments and those obtained by the sandwiched method (Takahashi and Kushiro, 1983).

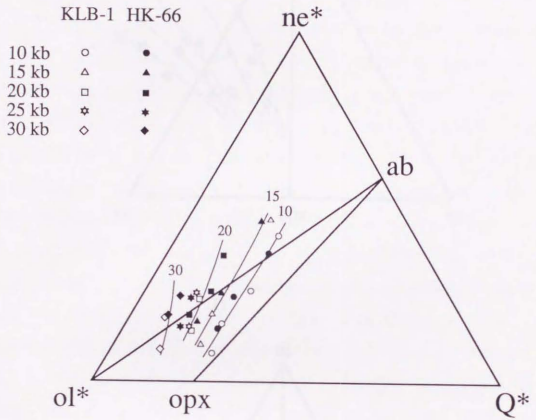

Fig. 8. Normative compositions of melts formed by partial melting of the two different lherzolites. After projection scheme described by Irvine and Baragar (1971); ne*=ne+0.6ab, Q*=Q+0.4ab+0.25opx, ol*=ol+0.75opx.

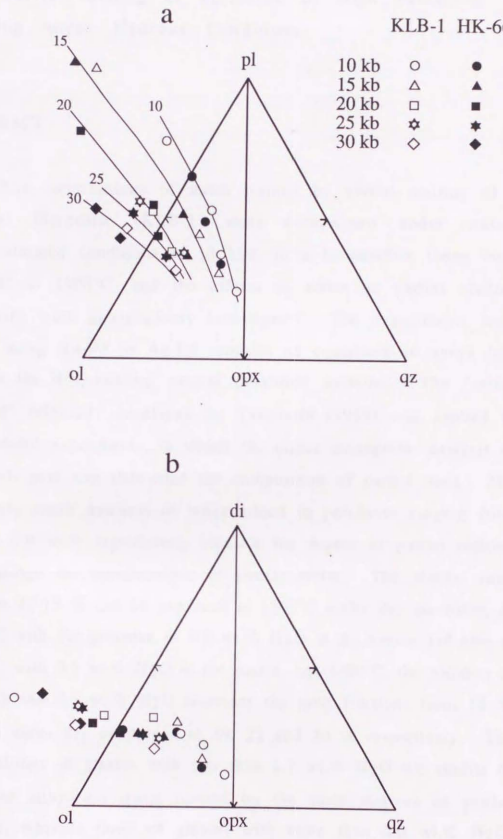

Fig. 9. Normative compositions of melts and the isobaric compositional trends defined by the present experiments in Walker's ternary projections (Walker et al., 1979). (a) projection from diopside onto the plane olivine-plagioclase-quartz (b) projection from plagioclase onto the plane olivine-diopside-quartz. Melts projected far away from the normative triangle were omitted in both projections.

III. Partial Melting of Peridotite at High Pressures; Batch Melting under Hydrous Conditions

ABSTRACT

The compositions of melts formed by partial melting of a natural lherzolite (KLB-1) were determined under water-undersaturated conditions at 10 kbar in a temperature range from 1100°C to 1300°C, and the effects of water on partial melting processes were quantitatively investigated. The experiments were made using Au-Pd or Ag-Pd capsules as containers to avoid iron loss in the H_2O-bearing natural peridotite systems. The "crimp method" originally developed by Takahashi (1989) was applied to the present experiments, in which the direct microprobe analysis of the melt pool can determine the composition of partial melt. The relatively small amounts of water added to peridotite ranging from 0.1 to 0.9 wt.% significantly increase the degree of partial melting and change the compositions of partial melts. The similar melt fraction 12-15 % can be produced at 1300°C under dry condition, at 1200°C with the presence of 0.2 wt.% H_2O in the source and also at 1100°C with 0.9 wt.% H_2O in the source. At 1300°C, the addition of 0.1, 0.2 and 0.5 wt.% H_2O increases the melt fractions from 12 % formed under dry conditions to 19, 22 and 30 % respectively. The compositions of glasses with less than 1.7 wt.% H_2O are similar to those of anhydrous melts formed by the same degrees of partial melting, whereas those of glasses with more than 6.0 wt.% H_2O formed at about 150°C below the dry solidus temperature are enriched in silica compared to the anhydrous melts. The effect of

water must be taken into account even for the genesis of tholeiitic basalts with wide range of water contents from 0.2 to 2.0 wt.%. The higher amounts of water in the source lherzolite for some hot spot regions such as Azores region along the Mid-Atlantic Ridge can be responsible for the relatively high degree of partial melting reflecting their relatively thick crustal thickness.

III-1. Introduction

Basaltic magmas are considered to be formed by partial melting of peridotite in the upper mantle and the melting experiments at high pressures are key to understand the genesis of basaltic magmas. Melt compositions formed under anhydrous conditions at high pressures have been successfully determined using a "diamond trap method" (session II) (e.g. Hirose and Kushiro, 1993; Baker and Stolper, 1993). However, the compositions of melts formed under the presence of water, particularly those of melts with less than 4 wt.% H_2O are still uncertain. The tholeiitic basalts have relatively low water abundances but some contain significant amounts of H_2O, ranging from less than 0.4 wt.% in mid-oceanic ridge basalts to up to 2 wt.% in back-arc basin basalts (e.g. Muenow et al., 1990). Their abundances are relatively low but water plays a significant role in their generation in the upper mantle as shown in this thesis.

There have been experimental difficulties in the melting experiments under water-bearing conditions mainly derived from the following problems. One is that in the Fe-bearing systems, significant Fe-loss is observed due to interaction of the samples

with the container. Second problem is that the melt compositions are modified at quenching. Kushiro (1990) determined nearly successfully the hydrous melt compositions formed by partial melting of a natural lherzolite, although it includes some problems still to be improved. In this experiments, Pt capsules saturated in iron prior to experiments were used as containers. However, the capsules were not fully satisfactory. The "sandwich method" was applied to avoid quench modification (e.g. Takahashi and Kushiro, 1983). And in his experiments, the H_2O abundances in quenched glass was always above 4 wt.% that cannot applied to the natural tholeiitic basalts which contain less than 2 wt.% H_2O.

In order to overcome these two problems, the present experiments were made with Au-Pd and Ag-Pd capsules as containers and with the "crimp technique" which was originally developed by Takahashi (1989). The Au-Pd and Ag-Pd capsules are suitable containers for the melting experiments for both Fe- and H_2O-bearing systems, which is reported in the separate paper (Kawamoto and Hirose, 1993). It is also necessary to make a melt pool to avoid the quench modification. Using the crimp technique, melt migrated to form a melt layer and its composition could be successfully determined by the direct microprobe analyses. The melt compositions and degrees of partial melting formed by partial melting of water-bearing natural lherzolite with 0.1-0.9 wt.% H_2O are presented here.

The previous melting experiments under hydrous conditions showed that the presence of water causes mainly two important effects on partial melting of peridotite; 1) it lowers the solidus temperature of the mantle peridotite and consequently degree of partial melting increases, and 2) the partial melt composition is

more silica-rich than the water-free melts. The main purpose of the present study is to estimate these effects quantitatively with a natural lherzolite and to discuss the genesis of water-bearing basaltic magmas in terms of melt compositions and degrees of partial melting.

III-2. Experimental technique

In the experiments reported here, two significant improvements were achieved compared to the previous melting experiments in both Fe- and H_2O-bearing systems. One is that $Au_{75}Pd_{25}$ and $Ag_{70}Pd_{30}$ capsules were used as containers at above 1200°C and 1100°C, respectively. Kawamoto and Hirose (1993) reported about Fe loss using their capsules that the relative loss of FeO* (total Fe as FeO*) from a water-undersaturated basaltic melt is less than 4 wt.% in a temperature range of 1100°-1300°C at 10 kbar. This is a comparative value to the analytical error of the microprobe. Second, the "crimp method" is applied to the present experiments on partial melting of peridotite. This technique has been originally developed by Takahashi (1989) for the melting experiments on amphibolite. It is needed to make a melt pool to determine the melt composition by the direct microprobe analysis without modification at quenching. The "diamond trap method" is quite useful for this purpose under anhydrous conditions, but it cannot be applied to the hydrous experiments because diamond easily reacts with water. Using the crimp technique, a melt accumulates and forms a melt layer without any stable crystals at the crimped part and along the inner curved surface of the

container. Figure 10 illustrates the present configuration and shows a SEM image of the melt layer. In both cases the thickness of the melt layer is more than 30 μm and sometimes above 100 μm, whereas less than 10 μm from the solid layer is affected by the overgrowth of adjacent minerals at quenching. Thus the melt composition can be determined by direct microprobe analysis of this layer. In the present experiments, the melt compositions were determined successfully formed by more than 7.9 % of degree of partial melting.

The starting material was a natural spinel-lherzolite from Kilborne Hole Crater in New Mexico designated KLB-1 which has been also used in the previous melting experiments by Takahashi (1986) and Hirose and Kushiro (1993) (session II). The present results, therefore, can be easily compared to those obtained under anhydrous conditions. Double-distilled water ranging 0.1-0.9 wt.% was added by a microcylinder to peridotite powder (5-30 μm in size) stored at 110°C. The total weight of the charges is about 100 mg except it is about 200 mg at run #30 with 0.1 wt.% H_2O addition. They were loaded in the $Au_{75}Pd_{25}$ capsules 5 and 4.7 mm in outer and inner diameter respectively and 15 mm in length. The capsules were crimped at their lower half and then sealed. Talc-pyrex outer sleeves and Alsimag inner sleeve and end lod were used. Only in run #28 the charge was loaded in $Ag_{70}Pd_{30}$ capsule, and salt-pyrex outer sleeves and graphite inner sleeve were used to lower oxygen fugacity. In this case graphite sleeve was completely insulated against the outer tapered graphite heater (Kushiro, 1976). In a run in which BN was used as the inner sleeve surrounding $Au_{75}Pd_{25}$ capsule, boron was detected in quenched glass and its compositions was very heterogeneous between the

separate melt pools. It must be cautioned that boron can migrate or diffuse through the $Au_{75}Pd_{25}$ capsule.

All the experiments were carried out with a piston-cylinder apparatus with 3/4 inch diameter assemblies at 10 kbar and at temperatures 1100°, 1200° and 1300°C. Calibration for pressure and other experimental procedures with this apparatus have been described elsewhere (Kushiro, 1976). Temperature was measured and controlled by $Pt/Pt_{90}Rh_{10}$ thermocouples. Analyses of the quenched melt layer were made with a scanning microprobe (JEOL JSM-840) with Link EDS system.

The runs were made for durations ranging from 23 to 66 hours (Table 7). In the sandwich experiments Kushiro (1990) showed that 24 hours and 8 hours are adequate for runs under water-saturated conditions at 1100°C and 1200°C respectively. The time needed for equilibration with the crimp method would be shorter than that for the sandwich experiments. The equilibration, therefore, is considered to be attained in the present study, although they were made under water-undersaturated conditions.

It is cared that hydrogen may be lost through the Au-Pd and Ag-Pd capsules during the runs. The loss of hydrogen probably causes the increase of ferric in charges, which results in the apparent partition coefficient (K_d) for Mg-Fe between olivine and melt assuming all Fe as Fe^{2+}. Its values in the present experiments, however, are 0.268-0.291 except run #27 which are similar to those in the anhydrous experiments about 0.3 (Table 8). In the run #32 the loss of 0.014 wt.% hydrogen leading the presence of about 1.1 wt.% Fe_2O_3 in charge results in the high Kd value more than 0.33. It suggests that the relative loss of H_2O is less than 26 % in the runs formed at 1300°C. Only in the run #27 made at 1100°C it

is significantly low, suggesting that significant amounts of hydrogen were lost in this run.

III-3. Results

All the runs were made under water-undersaturated conditions at temperatures 1100°, 1200° and 1300°C. 1100° and 1200°C are lower than the dry solidus temperature of KLB-1 at 10 kbar which is about 1250°C (Hirose and Kushiro, 1993). Details of the run conditions and the residual mineral assemblages are summarized in Table 7. Olivine, orthopyroxene and spinel are always present in the residue, whereas under anhydrous conditions spinel is eliminated at relatively low degree of melting >13%. It is due to the low oxygen fugacity in the anhydrous experiments using graphite capsule and it causes that Cr contents in anhydrous melts are higher than those in hydrous melts with the same melt fractions. Table 8 presents the analyses of quenched hydrous glass and also the compositions of anhydrous melts formed at 10 kbar from KLB-1 for comparison (Hirose and Kushiro, 1993). The degrees of partial melting are approximately estimated by calculation assuming that sodium is a perfectly incompatible element. In the present study, less than 0.03 wt.% Na_2O is resided in clinopyroxene, whereas the starting material contains 0.3 % Na_2O. The calculated degrees of melting range from 7.9 to 30.2 % in weight. The H_2O abundances in melt layers range from 0.5 to 6.3 wt.%, which are also estimated from the mass balance calculations.

At 1300°C, runs with three different amounts of H_2O in the chrages 0.1, 0.2 and 0.5 wt.% were made. All partial melts

containing 0.5, 0.9 and 1.7 wt.% H_2O (runs #30-#32) are high magnesian olivine tholeiites. With an increase of added water, the degrees of partial melting significantly increase from 12.1 % formed under dry conditions to 18.5, 21.8 and 30.2 % in the presence of 0.1, 0.2 and 0.5 wt.% H_2O in the source respectively. It is noted that the compositions and degrees of partial melting of the latter two glasses are quite similar to those formed at 1350° and 1400°C under anhydrous conditions respectively (runs #16 and #17). At 1200°C which is about 50°C below the dry solidus of KLB-1, a run was performed with 0.2 wt.% H_2O in the charge (run #29). Partial melt is also a high magnesian olivine tholeiitic basalts with 1.5 wt.% H_2O, and the calculated degree of partial melting is 13.7 %. It is also notable that both compositions and degrees of melting are similar to those formed at 1300°C under anhydrous condition (run #15). At 1100°C which is about 150°C below the dry solidus, runs were made with two different amounts of H_2O contents in lherzolite. With increasing H_2O added to peridotite from 0.5 to 0.9 wt.%, the degree of melting increases from 7.9 to 14.9 %. These partial melts (run #27 and #28) have significantly high H_2O content (6.3 and 6.0 wt.%) compared to melts formed at 1300° and 1200°C (run #29-32). Their compositions are olivine tholeiite (run #27) and quartz tholeiite (run #28). The melt with 6.3 wt.% H_2O is distinct from those in other runs in high FeO* and low TiO_2 contents due to its higher oxygen fugacity.

The compositions of these hydrous glasses are plotted on the Walker's ternary diagrams olivine-plagioclase-silica and olivine-diopside-silica (Figs. 11a and b). The 10 kbar melts formed under anhydrous conditions determined by Hirose and Kushiro (1993) are also shown for comparison, which form an isobaric univariant curve

on these diagrams. Kushiro (1990) showed that the isobaric univariant curve for melts with 4.4-6.6 wt.% H_2O shifts away from the olivine apex and are close to that under dry conditions at lower pressures. In the present study the compositions of melts with less than 1.7 wt.% H_2O formed at 1200° and 1300°C are plotted very close to the univariant curve under anhydrous conditions formed at the same pressure. On the other hand, those of melts formed at 1100°C which is lower by about 150°C than the dry solidus temperature are plotted apart from that univariant line, and are significantly enriched in silica compared to melts formed under dry conditions and by the same degrees of partial melting.

III-4. Changes in degree of melting and melt composition by the effect of water

The present results show that the presence of small amounts of H_2O significantly increases the degrees of partial melting of lherzolite and changes the melt compositions formed. Figure 12 displays the change in degree of melting with increasing temperature and amount of water added to peridotite. The solidus temperature of lherzolite KLB-1 is just below 1250°C; however, the presence of 0.5 wt.% H_2O lowers it to less than 1100°C and results in the degree of melting at 1100°C comparative to that formed at 1250°C under anhydrous condition. The melt fractions of 12-15 % which are produced at 1300°C under dry condition can be formed at 1200°C with 0.2 wt.% H_2O in the lherzolite and also at 1100°C with 0.9 wt.% H_2O.

Figure 13 shows the oxide contents in both hydrous and anhydrous glasses formed at 10 kbar as a function of degree of partial melting. It is noted that the oxide contents of melts with less than 1.7 wt.% H_2O are generally similar to those of anhydrous melts formed by the same degrees of partial melting. On the other hand, melts with 6.0 and 6.3 wt.% H_2O formed at about 150°C below the dry solidus temperature are distinctly lower in MgO and higher in SiO_2 contents than those formed under the dry conditions.

The changes in melt fraction and composition with increasing H_2O content at constant temperature can be estimated in the runs made at 1300° and 1100°C. With an increase of water at both temperatures, the melt fraction increases significantly as presented above (Fig. 12), and the compositional change of melts is similar to that of melts formed with increasing temperatures under anhydrous conditions. The change in MgO and Al2O3 contents are shown in figure 14. It is nearly parallel to the isobaric univariant line under dry conditions in the ternary diagram (Fig. 11).

The compositional change of melt with increasing temperature formed from a lherzolite with constant H_2O content is shown from the runs made at 1300° and 1200°C with addition of 0.2 wt.% H_2O and from the runs formed at 1300°C and 1100°C with addition of 0.5 wt.% H_2O. In the runs with 0.2 wt.% H_2O in the lherzolite, the compositions of partial melts (runs #29 and #31) are plotted close to the anhydrous univariant curve in the ternary diagram and change similarly to anhydrous melts with increasing temperature, reflecting their relatively low H_2O contents (less than 1.7 wt.%). On the other hand, in the runs with addition of 0.5 wt.% H_2O, water contents in both melts (runs #27 and #32) are significantly

different and the compositional change is not parallel to the univariant curve under dry conditions (Fig. 11a).

The present experiments at 1300°C show that the melt fraction and composition similar to those of anhydrous melt formed at 1350°C are produced by addition of 0.2 wt.% H_2O in the charge and, in the same way, the addition of 0.5 wt.% H_2O results in the melt fractions and compositions similar to those of melts formed at 1400°C under dry condition. Those of melt formed by addition of 0.1 wt.% H_2O are between those of anhydrous melt and melt produced by addition of 0.2 wt.% H_2O. Also, the presence of 0.2 wt.% H_2O at 1200°C forms melt fraction and composition similar to those of anhydrous melt formed at 1300°C.

III-5. Partial melting of hydrous mantle and basaltic magma genesis

Water is most probably always present when the basaltic magmas are generated in the upper mantle, although its amount is not large. The melt fractions and compositions produced from the hydrous peridotite have little been estimated quantitatively (Green, 1973; Kushiro, 1990). The present experiments show that the presence of water significantly increases the melt fractions and that the compositions of melts with less than 1.7 wt.% H_2O are fairly similar to those of anhydrous melts with the same melt fractions.

The H_2O contents in tholeiitic basalts are generally low; however some contain up to 2.0 wt.% and the effects of water can be significant. They are widely ranged depending on different tectonic settings; 0.1-0.3 wt.% for N-MORB (Delaney et al., 1978),

0.2-2.0 wt.% for back-arc basin basalts (Garcia et al., 1979; Muenow et al.,1980; Danyushevsky et al., 1993), 0.3-0.7 wt.% for oceanic island tholeiites (Muenow et al., 1990) and as small as 1 wt.% for island arc tholeiites (Garcia et al., 1979; Sakuyama, 1979). Even such small amounts of H_2O (e.g., less than 2 wt.%) in melts can influence significantly on their generation as shown in the present experiments. The melt with 0.9 wt.% H_2O formed at 1300°C, for example, are similar to the anhydrous melt formed at 1350°C in compositions and melt fractions (Table 8).

The "hot spot" region on the Mid-Atlantic ridge (MAR) are distinguished from normal ridges by their shallower water depths which are caused by thick crustal thickness (Klein and Langmuir, 1987). It reflects relatively higher degrees of partial melting in the hot spot regions as also evidenced by the depleted compositions of dredged peridotites (Michael and Bonatti, 1985). Primitive glasses (MgO > 8%) from these hot spot regions have generally high H_2O contents 0.5-0.7 wt.% at Azores region, whereas those in primitive glasses from normal ridges are 0.2-0.4 wt.% (Jambon and Zimmermann, 1990; Delaney et al., 1978; Schilling et al, 1983). The relatively high degrees of partial melting in the upper mantle along the MAR could thus reflect also the higher amounts of H_2O in the source peridotite. The primitive N-MORBs can be formed approximately at 10 kbar and 1300°C based on the batch melting model (e.g. Fujii and Bougault, 1983; Fujii and Scarfe, 1985; Hirose and Kushiro, 1993). The present experiments show that the presence of 0.1 wt.% H_2O in the source lherzolite can produce an oceanic crust thicker by 50 % than that formed from an anhydrous lherzolite with melt containing 0.5 wt.% H_2O under these pressure-temperature conditions. The 0.5-0.7 wt.% H_2O in primitive basalts

can be responsible for relatively thick oceanic crust (about 8 km) at the Azores region along the MAR compared to the crust of normal mid-oceanic ridge which is about 6 km thick at MAR approximately 45°N (Searle, 1976; Lewis and Snydsman, 1979).

The major element compositions of glasses from the hot spot regions along the mid-oceanic ridges could be explained by that they were formed by relatively higher degrees of partial melting from the anhydrous peridotite (see Fig. 2 in Klein and Langmuir (1987)). The present experiments demonstrated that melts with less than 1.7 wt.% are similar in composition to the anhydrous melts formed by the same degrees of partial melting. Therefore, the assumption that the presence of higher amounts of H_2O mainly causes their higher degrees of partial melting is consistent with the observations by Klein and Langmuir.

Basalts from the back-arc basin generally contain relatively large amounts of H_2O up to 2 wt.% (Muenow et al., 1980). Hawkins et al.(1990) suggested that the parental Mariana Trough basalts are similar to the primitive MORB in terms of major elements, but they have 0.5-1.5 wt.% H_2O. The crustal thickness of this basin is about 5 km which is comparable to that of normal mid-oceanic ridges (LaTraille and Hussong, 1980). The primitive N-MORBs and parental Mariana Trough basalts can be formed approximately at 10 kbar and 1300°C under anhydrous conditions based on the batch melting model, whereas a melt with 1.5 wt.% H_2O with similar melt fraction and composition can be produced at 10 kbar and 1200°C. It implies that the primary Mariana Trough magmas were formed at temperatures lower by about 100°C than those at normal mid-oceanic ridges.

TABLE 7. Details of runs

Run #	P (kbar)	T (°C)	Duration (hr)	H2O added (wt.%)	Residue
27	10	1100	65.6	0.5	ol, opx, cpx, sp
28	10	1100	47.9	0.9	ol, opx, cpx, sp
29	10	1200	65.0	0.2	ol, opx, cpx, sp
30	10	1300	27.6	0.1	ol, opx, cpx, sp
31	10	1300	29.8	0.2	ol, opx, cpx, sp
32	10	1300	23.3	0.5	ol, opx, sp

TABLE 8. Compositions of melt pools (recalculated as 100% anhydrous)

Run	27	28	29	30	31	32
P (kbar)	10	10	10	10	10	10
T (°C)	1100	1100	1200	1300	1300	1300
H2O added	0.5	0.9	0.2	0.1	0.2	0.5
SiO2	52.47	51.84	49.50	49.20	50.81	52.39
TiO2	0.73	0.74	0.67	0.57	0.53	0.31
Al2O3	19.66	18.36	18.70	15.55	13.60	12.29
FeO*	6.66	6.68	6.56	7.46	7.91	8.32
MnO	0.09	0.17	0.12	0.18	0.14	0.16
MgO	7.30	9.13	10.46	12.56	13.91	16.21
CaO	9.19	10.98	11.74	12.69	11.55	9.07
Na2O	3.80	2.01	2.18	1.62	1.38	0.99
K2O	0.08	0.04	0.04	0.06	0.03	0.06
Cr2O3	0.02	0.04	0.04	0.11	0.15	0.21
Total	100.00	100.00	100.00	100.00	100.00	100.00
H2O in melt†	6.3	6.0	1.5	0.5	0.9	1.7
Fo mole %	91.3	90.1	90.7	91.5	91.5	92.3
Kd (Fe/Mg)	0.186	0.268	0.291	0.282	0.291	0.290
F††	7.9	14.9	13.7	18.5	21.8	30.2

†; H2O contents in melts are estimated from the melt fractions
††; degree of partial melting calculated from Na2O abundance

a.

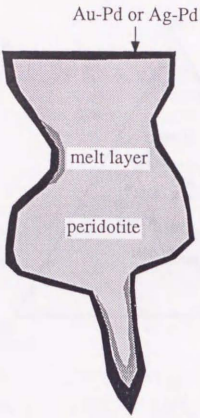

b.

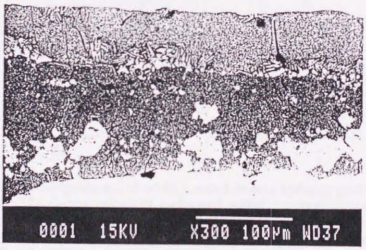

Fig. 10. (a) The configurations of charges in the present experiments applying the crimp method. Melt layers are formed at the crimped part and along the inner surface. (b) Backscattered electron image of a charge showing the melt layer without any stable crystals.

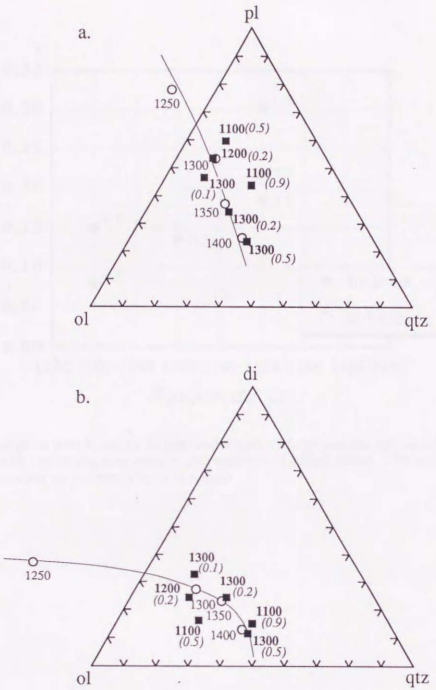

Fig. 11. Normative compositions of melts formed from a hydrous peridotite at 10 kbar (closed square). The compositions of melts and isobaric univariant curve for the dry conditions at 10 kbar are also shown for comparison (session II) (open circle). Each plain number indicates temperature condition and italic number indicates the amounts of added water in the source. (a) projection from diopside onto the plane olivine-plagioclase-quartz (b) projection from plagioclase onto the plane olivine-diopside-quartz. Note that melts formed at 1200° and 1300°C with less than 1.7 wt.% H_2O are plotted on the univariant curve for the anhydrous conditions.

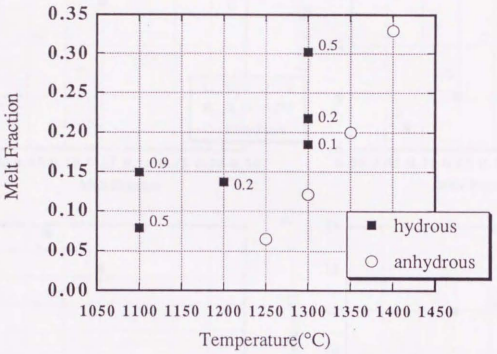

Fig. 12. Change in melt fractions formed under both hydrous and anhydrous conditions at 10 kbar with increasing temperature and amounts of added water. The amounts of water in the source are presented by % in weight.

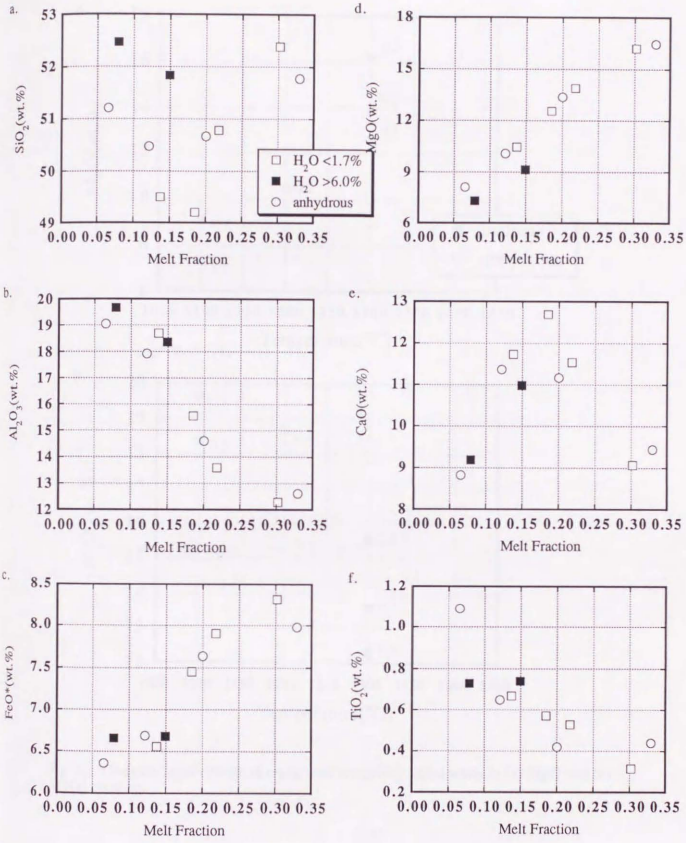

Fig. 13. Compositional change of melts with increasing melt fractions in (a) SiO_2, (b) Al_2O_3, (c) FeO*, (d) MgO, (e) CaO and (f) TiO_2 contents. Melts with less than 1.7 wt.% H2O are similar in composition to anhydrous melts with the same melt fractions. On the other hand, those with more than 6.0 wt.% H_2O formed at 1100°C are enriched in SiO_2 and depleted in MgO contents.

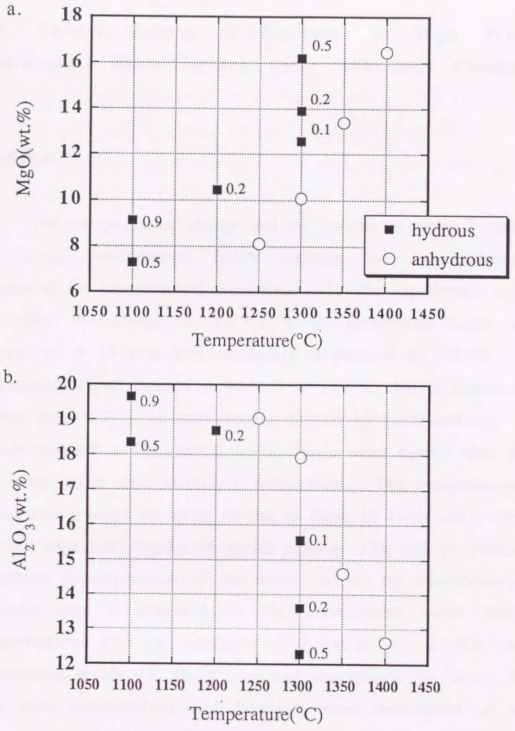

Fig. 14. Compositional change of melts with increasing added water in (a) MgO and (b) Al_2O_3 contents.

IV. Partial Melting of Peridotite at High Pressures; Incremental Batch Melting under Anhydrous Conditions

ABSTRACT

The compositional change and the volume of melts formed by non-modal incremental batch melting were experimentally examined for two different conditions. (1) The experiments with a complete withdrawal of 3.0-9.8 wt.% incremental melts were performed at 15 kbar with increasing temperature to 1425°C. The accumulated melt fraction is 22.8 % at 1425°C that is significantly lower than 36.7 % of melt fraction formed by batch melting. The oxide contents in incremental melts change more rapidly than those in batch melts with increasing temperature. The compositions of accumulated melts are quite similar to those of batch melts formed by the same total degrees of partial melting. (2) Melt generation by adiabatic decompression of the mantle within the one-dimensional column was investigated by the incremental batch melting experiments with a complete withdrawal of 4.4-6.4 wt.% increments at 20, 15, 10, 5 kbar and atmospheric pressure. Both the melt compositions and fractions were determined at high pressures, and only melt fraction was estimated at atmospheric pressure. It is notable that the rate of melt production decreases with decreasing pressure and that only quite small amounts of melt are produced at depths shallower than 30 km. The accumulated composition of incremental melts formed in a pressure range from 20 kbar to atmospheric pressure is similar to that of batch melt formed at 15 kbar.

IV-1. Introduction

The recent theoretical, experimental and geochemical studies suggest that small fractions of melt can segregate from the host peridotite and that melts are formed by near fractional melting (e.g. Mckenzie, 1984; Riley and Kohlstedt, 1991; Johnson et al., 1990; Gill and Condomines, 1992). Melting experiments are key to understand the magma generation in the upper mantle; however, the previous experiments have been emphasized the batch melting processes. Therefore, the numerous modelling of magma generation by the fractional melting has been attempted, but they were still uncertain about the melt fractions and compositions (Klein and Langmuir, 1987; Mckenzie and Bickle, 1988; Niu and Batiza, 1991; Kinzler and Grove, 1992b).

The melt compositions formed by fractional fusion in the simple systems were shown by Presnall (1969) from the geometry of the phase diagram. Recently Kinzler and Grove (1992a,b and 1993) proposed the method of integration to calculate the melt compositions formed by near fractional melting of lherzolite. The degree of partial melting, however, cannot be predicted by their integrations. The determination of the degree of partial melting is quite important to estimate the melt volume produced and the compositions of accumulated melts. The temperatures of the source mantle were estimated from the thickness of oceanic crust at mid-oceanic ridges (Klein and Langmuir, 1987; Mckenzie and Bickle, 1988). Their estimations, however, were based on the batch melting experiments and therefore, the similar estimation for the melt generation by incremental batch melting should be made.

To aim further understanding of the magma generation by near fractional melting or incremental batch melting processes, melt generation by non-modal incremental batch melting was experimentally investigated in this study. The experiments were made (1) at 15 kbar with increasing temperature to 1425°C, and (2) at 20, 15, 10, 5 kbar and atmospheric pressure to simulate the melt generation by adiabatic decompression of the mantle. The compositions and fractions of incremental melts are presented here and those formed by batch melting are also shown for comparison. Melt generation by incremental batch melting and the differences from batch melting process are discussed in this session.

IV-2. Experimental technique

2.1 Starting material

Both isobaric and decompressional incremental batch melting with complete melt withdrawal were experimentally performed in this study. The first incremental melts in both experiments were referred to the results by Kushiro (1993) which were obtained from a garnet lherzolite from Thaba Patsoa kimberlite in Lesotho designated PHN-1611 (Nixon and Boyd, 1973; Smith et al., 1993). Its composition is shown in Table 9 that has a primitive mantle characteristics in terms of major elements except K_2O (Sun and McDonough, 1989). Relatively high K_2O content (0.14 wt.%) is favorable to estimate the degree of partial melting because K_2O could be assumed to be a perfectly incompatible element at least below 20 kbar.

In the present non-modal melting experiments, gel was prepared for the starting materials with peridotitic compositions. The composition of each starting material was calculated for Si, Ti, Al, Fe, Mg, Ca, Na, K and Cr from degree of partial melting and composition of each incremental melt formed in one-step before the experiments. About 0.1 wt.% K_2O was always doped to estimate the degree of partial melting. The analyses by XRF (Phillips PW1480) and the differences from the calculated compositions are listed in Table 9. The gel is a suitable starting material compared to the natural peridotites or oxide mixtures because it is quite easy to react. Only run #40 was made on garnet lherzolite PHN-1611 at 5 kbar in this study.

2.2 Experimental technique and run conditions

The compositions of melts were determined by the "diamond aggregate method" in this study (e.g. Hirose and Kushiro, 1993; Baker and Stolper, 1993; Kushiro, 1993). The experimental technique same as that used by Hirose and Kushiro (1993) and Kushiro (1993) was applied to the present experiments and the configurations of charges were also the same. A few small chips of loosely sintered aggregates (200-800 μm across) of diamond powder (40-60 μm in diameter) were placed between the peridotite layer to separate the melts from the host peridotite into the pore space between the diamond aggregates. It is necessary that the pore space between the diamond grains is smaller than the melt volumes formed; otherwise significantly lower-pressure melts are obtained (Kushiro and Hirose, 1992). In the present experiments the volume of diamond chips is less than 3 % of

peridotite. The volume of the pore space between the aggregates is less than 50 % of the chips, so that the pore space is about 1.5 volume % of the charges.

The gel was heated at 850°C at oxygen fugacity for wüstite stability condition for about 12 hours to be dehydrated prior to experiments. It was loaded into graphite capsules (2 mm in diameter and 3.5 mm in length) with the sintered diamond chips and were sealed in the Pt capsules. The lherzolite was ground to a 10-30 μm powder and was loaded into the graphite capsule, which was heated at 1000°C and at fO_2 of 10^{-14} atm for 3 hours to dehydrate, and then it was processed similarly to the gels. Before temperature increases to above the solidus, the gel was always sintered at just below the solidus temperature for 1 hour under high pressures. All the high-pressure experiments were conducted with a piston-cylinder type apparatus. Calibration for pressure and other experimental procedures with this apparatus have been described elsewhere (Kushiro, 1976). Temperature was measured and controlled by $Pt/Pt_{90}Rh_{10}$ thermocouples. The run under atmospheric pressure was made by a gas-mixing furnace at 1235°C and at fO_2 of 10^{-9}.

The isobaric experiments were made at 15 kbar and at temperatures 1275°, 1350°, 1400° and 1425°C with a complete withdrawal of incremental melts. The decompressional experiments were made at 20, 15, 10, 5 kbar and atmospheric pressure to simulate the melt generation by roughly adiabatic step-wise decompression of the mantle within one-dimensional melting column with a complete melt withdrawal at each pressure. Temperatures were calculated from the melt fraction, latent heat of fusion for mantle peridotite (130 cal/g), the heat capacity (0.3

cal/g) for both melt and solid and the adiabatic gradient of the mantle (0.6 °C/km) (Kinzler and Grove, 1992b; Mckenzie and Bickle, 1988). They ranged from 1350° to 1235°C in the present experiments. The temperature conditions in the experiments are slightly different from the calculated conditions and the differences are also presented in Table 10.

Run durations of high-pressure experiments ranged from 23 to 71 hours at temperatures above 1300°C and from 44 to 77 hours at temperatures below 1200°C. The duration of atmospheric pressure experiment was 45 hours. The equilibration is probably attained in shorter run durations than the previous experiments with the diamond aggregate method using natural lherzolites (Johnson and Kushiro, 1992; Hirose and Kushiro, 1993), and present run durations are adequate for equilibration according to the previous studies in which the time needed for equilibrium was examined by changing run durations.

After quenching, the charges were polished and the trapped melts between the diamond aggregates were analyzed by a scanning microscope (JEOL JSM-840) with Link EDS system. The compositions can be determined without quench modification. The size of constituent minerals are generally less than 10 μm in diameter and the compositional zoning in minerals is minimum in runs using gel starting materials, suggesting that the bulk equilibrium was nearly attained in the present experiments.

IV-3. Experimental results

The detailed run conditions and the residual solid assemblages are summarized in Table 10. The compositions of melts and the calculated degrees of partial melting are shown in Tables 11 and 12.

3.1. Effects of doped K_2O

The degree of partial melting of each incremental melt was determined by the mass balance calculations based on doped K_2O contents assuming the perfect incompatibility to solid. The doping of K_2O to peridotites increases the degree of partial melting and modifies the compositions of partial melts probably to enrich SiO_2 content. The abundances of doped K_2O content, however, were less than 0.1 wt.% in all the runs, which may not influence significantly partial melting. The effect of 0.1 wt.% K_2O may be similar to that of 0.02 wt.% H_2O which corresponds to the same mole %. The hydrous melting experiments show that melt fractions and compositions formed at 1200° and 1300°C with 0.2 wt.% H_2O in the source are similar to those of anhydrous melts formed at 1300° and 1350°C respectively (session III, Table 8). It implies that the effect of doping may be comparable to that of an increase of temperature by 5-10°C. It is much smaller than the present temperature intervals.

3.2 Isobaric incremental batch melting

3.2.1 Degrees of partial melting

Figure 15 shows the total degrees of partial melting with increasing temperature by incremental batch melting. Those formed by batch melting in Kushiro (1993) are also presented for comparison. The first incremental melt were formed at 1275°C by 9.9 % of partial melting of lherzolite. With increasing temperature, the accumulated melt fraction increases by both melting processes, but that formed by incremental batch melting are significantly lower than that formed by batch melting at same temperatures. The melt fraction formed from the residue at 1275°C was too small to be detected at 1325°C, and as less as 3.9 % melt fraction was produced at 1350°C where the total degree of partial melting is 13.5 % by incremental batch melting and 20.7 % by batch melting. Such difference is largest at 1425°C in the present study; 22.8 % by incremental batch melting and 36.7 % by batch melting.

The smaller melt fractions formed by incremental batch melting probably reflect the following two effects; (1) the compositions of source peridotite become depleted due to melt withdrawal, and (2) augite changes into subcalsic augite with increasing temperature. The temperature-melt fraction curve for the batch melts (Fig. 15) has a break where the slope of curve changes corresponding to elimination of solid phases (Kushiro, 1993), and the melt fraction increases significantly before the break. This curve for incremental melts shows that the rate of melt generation is relatively low between 1275° and 1325°C corresponding to the change of solid phases from augite to subcalsic augite. The differences in melt fractions formed by both the melting processes at same temperatures are largest at such breaks and relatively small between them.

3.2.2 Compositional change of melts

Figure 16 shows the variations of oxides in batch melts, incremental melts and accumulated incremental melts as a function of accumulated melt fractions (total degrees of partial melting). The accumulated incremental melt at 1350°C, for example, consists of incremental melts formed at 1275° and 1350°C. The SiO2 content in incremental melts decreases and then increases with a weak minimum at 13.5 % accumulated melt fraction (Fig. 16a). The TiO_2, Al_2O_3 and Na_2O contents in incremental melts decrease with increasing melt fractions more rapidly and show apparently lower values than those in batch melts with the same melt fractions (Figs. 16b, f and g). Both the TiO_2 and Na_2O contents in melt with 22.8 % accumulated melt fraction are higher than those in melt at 19.8 %. It is probably caused by the analytical error of quenched glass due to their low concentrations. The FeO and MgO contents increase monotonically with increasing melt fractions (Figs. 16c and d), and the CaO content increases and then decreases with a sharp maximum at 19.8 % accumulated melt fraction (Fig. 16e). The contents of FeO, MgO, SiO_2 (above 13.5 % accumulated melt fraction) and CaO (below 19.8 % accumulated melt fraction) increase more rapidly and show higher values than those in batch melts with the same melt fractions. It is notable that the accumulated incremental melts are quite similar in all of these oxide contents to batch melts formed by the same total degrees of partial melting.

The compositions of batch melts, incremental melts and accumulated incremental melts are plotted on the ternary diagrams olivine-plagioclase-silica (Fig. 17). The abundances of doped K_2O in incremental melts and accumulated incremental melts were ignored

for this plot. The compositions of accumulated incremental melts are close to the isobaric "univariant curve" for batch melts, which moves toward the orthopyroxene apex with increasing total degrees of partial melting. The compositions of incremental melts are enriched in orthopyroxene component compared to batch melts, and that of incremental melt formed at 1425°C has normative quartz.

The compositional similarity between both melts results in the similar bulk compositions of residual solids at the same melt fractions except a slight difference is observed in CaO contents. The temperatures to produce same melt fractions, however, are significantly different, reflecting in the compositions of residual solid phases, and the residual phase assemblages are sometimes different (Table 10).

3.3 Decompressional incremental batch melting

The decompressional incremental batch melting was experimentally investigated to simulate melt generation from the adiabatically upwelling mantle which intersects the solidus at about 22.5 kbar. The compositions and fractions of incremental melts were determined in the present experiments except only melt volume fraction was estimated in the atmospheric pressure experiment by modal analysis. Olivine-orthopyroxene-clinopyroxene were always present as the residual solid phases. Melt generation by batch melting is also considered for comparison at the same pressure-temperature conditions. The compositions and fractions of batch melts were refereed to Kushiro (1993). Those of melt formed at 15 kbar and 1311°C were inferred from

the results at 1325° and 1300°C, and those at 10 kbar and 1276°C were substituted by the results at 1275°C.

3.3.1 Degrees of partial melting

Figure 18a shows the accumulated melt fractions formed by both incremental batch melting and batch melting as a function of pressure. The accumulated melt fraction by incremental batch melting increases with progressive pressure release. It is notable, however, that the rate of melt production decreases from 22.5 kbar to lower pressures and that only quite small amounts of incremental melt (about 1.3 % in volume) were formed at depths shallower than 30 km. Similarly to the incremental batch melting, the rate decreases from 22.5 to 5 kbar. The melt fractions formed by incremental batch melting are always higher than those formed by batch melting; 12.6 % for the former whereas 17.4 % for the latter at 15 kbar, and 16.9 % and 21.5 % respectively at 10 kbar.

3.3.2 Compositions of melts

Figure 19 shows the oxide variations in batch melts, incremental melts and accumulated incremental melts as a function of pressure. The accumulated incremental melt at 15 kbar, for example, is a melt accumulated from incremental melts formed at 20 and 15 kbar. The SiO2, Al2O3, FeO and MgO contents in accumulated melts are different from those of batch melts with the same melt fractions at each pressure due to their strong dependence on pressure (Hirose and Kushiro, 1993; Kushiro, 1993). On the other hand, CaO, TiO_2 and Na_2O contents in accumulated

melts are similar to those in batch melts formed by the same degrees of partial melting. The SiO_2 contents in incremental melts increase monotonically with decreasing pressure. Their accumulated contents are significantly lower than those in batch melts at the same pressures (Fig. 19a). The Al_2O_3, TiO_2 and Na_2O contents in incremental melts decrease monotonically with successive melt formation (Figs. 19b, f and g). The accumulated TiO_2 and Na_2O contents are higher than those in batch melts at the same pressures due to lower degrees of partial melting than batch melts. On the other hand, the accumulated Al_2O_3 contents are slightly lower than those in batch melts. The FeO contents in incremental melts are maximum at 15 kbar and then decrease to 10 kbar, whereas those in batch melts decrease monotonically (Fig. 19c). The accumulated FeO contents are nearly constant and always higher than those in batch melts. The MgO contents in incremental melts are also maximum at 15 kbar and then decrease similarly to those in batch melts (Fig. 19d). The accumulated MgO contents increase slightly with increasing melt fractions and significantly higher than those in batch melts at 5 kbar. The CaO contents in incremental melts increase monotonically with increasing melt fractions, but accumulated contents are significantly lower than those in batch melts (Fig. 19e).

The compositions of batch melts, incremental melts and accumulated incremental melts are plotted on the ternary diagram olivine-plagioclase-silica (Fig. 20). The compositions of accumulated incremental melts are significantly different from those of batch melts at each pressure showing depletion in silica component. The incremental melt accumulated from 20 to 5 kbar and probably that

accumulated to atmospheric pressure are close in composition to batch melt formed at 15 kbar.

IV-4. Magma generation by incremental batch melting of peridotite

The recent studies on magma generation in the upper mantle suggest that the degrees of partial melting and the compositions of partial melts are controlled by near fractional melting processes at mid-oceanic ridges (e.g. Mckenzie, 1984 and 1985; Riley and Kohlstedt, 1991; Johnson et al., 1990; Sobolev and Shimizu, 1993). Magma generation by incremental batch melting or near fractional melting process is discussed based on the present results.

4.1 Melt volume formed by incremental batch melting of peridotite

The present results show that the volume of melt formed by the incremental batch melting process is significantly smaller than that formed by the batch melting process. The difference is generally larger with increasing total degrees of partial melting. It is possible, therefore, that when melts were formed at higher temperatures the difference in volume of melts formed by the different melting processes is larger. And if melt generation is controlled by the near fractional melting process where much smaller volume of melts segregate than that of present incremental melts (3.7-9.8 % melt fractions), the differences from the batch melting process could be larger.

The thickness of oceanic crust is considered to reflect the volume of melts formed by partial melting of the source mantle peridotite. The temperatures of the mantle to generate magmas within the upwelling melting column at mid-oceanic ridges were estimated from the thickness of oceanic crusts (Mckenzie, 1984; Klein and Langmuir, 1987; Langmuir et al.,1992; Kinzler and Grove, 1993). Their estimations, however, depend on the degree of partial melting determined by the batch partial melting experiments, which must be significantly different from those in the near fractional melting process. The present experimental results on incremental batch melting suggest that the melt fractions formed by fractional melting can be significantly smaller than those formed by batch melting (Figs. 16 and 18a).

The rate of melt production by pressure release is a complex function of pressure, but was approximated to be a constant value; for example, 1.2 % melt production per kilobar based on batch partial melting experiments (Ahern and Turcotte, 1979; Klein and Langmuir, 1987; Langmuir et al.,1992; Kinzler and Grove, 1993). Mckenzie and Bickle (1988) also estimated the melt fractions as a function of temperature normalized to the solidus and liquidus temperatures. The melting experiments with less than 15 % melt fractions has been insufficient and therefore, their estimations of melt production by batch melting are uncertain where the melt fraction is relatively small. Kushiro (1993) determined the change of melt fractions formed by batch melting over the wide range of pressure-temperature conditions. He showed that the volume of melt produced is a complex function of pressure. In the present decompressional incremental experiments, the pressure versus accumulated melt fraction diagram (Fig. 18a) shows that the rates

of melt production by both incremental batch melting and batch melting are not constant but significantly decrease from 22.5 kbar to lower pressures. It is notable that only small amounts of melt are produced at pressures lower than 10 kbar by both the melting processes; 17.1 wt.% of melt fraction is formed at pressures higher than 10 kbar, whereas only about 1.3 vol.% of melt fraction is produced at pressures lower than 10 kbar.

The crustal thickness at mid-oceanic ridges depends on the sum of total degrees of partial melting formed at different depths within the melting column. The sum of them formed by incremental batch melting within the one-dimensional melting column in a pressure range from 22.5 kbar to atmospheric pressure is similar to the estimation using 1.2 % per kilobar of a constant rate of melt production (Ahern and Turcotte, 1979), although the rate is quite different (Fig. 18a). And it is lower by about 20 % than that formed by batch melting in the present modelling. When the melts are generated within the one-dimensional upwelling melting column from about 22.5 kbar to atmospheric pressure, the thickness of residual oceanic crust is 10.5 km by setting the crustal density 2.95 g/cm^3 (Klein and Langmuir, 1987).

4.2 Compositions of melts formed by incremental batch melting of peridotite

The isobaric melting experiments show the compositional similarities between batch melts and accumulated incremental melts formed by the same total degrees of partial melting (Figs. 16 and 17), which are also inferred from the geometry of phase diagram in the simple system (Presnall, 1969). Melts with similar

compositions can be formed by both incremental batch melting and batch melting processes. The temperature conditions of their formation, however, are significantly different; the melt with 13 % fraction is generated at 1350°C by incremental batch melting and is also formed at about 1287°C by batch melting (Fig. 16). When the melts are formed by increasing temperature of the source, their volume and composition depend on the melting process. It is possible that some calc-alkaline andesites were formed by partial melting of the lower crust (e.g. Rushmer, 1991). Their estimation of melting temperatures based on batch melting could be lower estimates if the melt generation was controlled by the incremental batch melting process. The different melting processes result in the different compositions of residual phases. The present experiments show that subcalsic augite and pigionite have an important role when melts are generated by increasing temperature in the upper mantle.

The compositions of accumulated incremental melts formed by decompressional melting are significantly different from those of batch melts (Figs. 18a-g). The oxides whose contents in partial melts are strongly dependent on pressure such as SiO_2, Al_2O_3, FeO and MgO are significantly different in both melts.

Recently melt formation by near fractional melting process over a wide pressure range at mid-oceanic ridges has been discussed. It should be stressed from the present experimental results on decompressional incremental batch melting process that the rate of melt production decreases from 22.5 kbar to lower pressures, and melts are hardly produced at pressures lower than 10 kbar. It causes that the compositions of accumulated incremental melts formed within the melting column strongly

reflect those of increments formed at pressure higher than 10 kbar (Fig. 20). The volume of melt formed within the melting column estimated from the present experimental results is close to that calculated by setting the rate of melt production 1.2 % per kilobar based on the results of batch melting experiments (Ahern and Turcotte, 1979), which was used in the modelling by Klein and Langmuir (1987) and was similar to that used in Mckenzie and Bickle (1988). Mckenzie and Bickle (1988) discussed that the upwelling mantle with potential temperature 1280°C forms the normal oceanic crust which is 7 km thick and generates melt which is similar in composition to the primitive mid-oceanic ridge basalts (MORBs) based on the results of batch melting experiments. Such observations in the present experiments are consistent with their estimation of potential mantle temperature, but suggest that the compositions of parental MORBs are different from those of primitive MORB suite, for example, depleted in SiO_2 content reflecting the compositions of incremental melts formed at relatively high pressures.

It is controversial, however, that the primitive mid-oceanic ridge basalts (MORBs) are similar in composition to batch melts formed by partial melting of peridotite at 10 kbar (e.g. Fujii and Scarfe, 1985; Fujii, 1989; Hirose and Kushiro, 1993; Kushiro, 1993). The steady-state melt formation process can be controlled by the batch melting process even when small fractions of melt segregate from the host peridotite within the one-dimensional melting column, because the sum of melt and solid flux is constant at each depth. The compositional similarity of primitive MORB suite to 10 kbar batch melts may suggest the melt formation is controlled by batch melting processes at pressures higher than 10 kbar, where

small fractions of melts segregate from the host peridotite and re-equilibrate during their migration with the surrounding peridotite (Hirose and Kushiro, 1993). The present experimental observation that melts are hardly formed at pressures lower than 10 kbar may explain the rareness of primitive basalts with normative quartz (Presnall and Hoover, 1987; Sobolev and Shimizu, 1993).

TABLE 9. Compositions of starting materials

isobaric experiments

	PHN 1611†	gel-1††	gel-2	gel-3
SiO2	44.60	44.21 (+0.17)†††	43.45 (-0.56)	42.84
TiO2	0.26	0.11 (+0.01)	0.06 (±0.00)	0.02
Al2O3	2.81	1.24 (+0.06)	0.74 (+0.01)	0.19
FeO*	10.26	10.55 (+0.03)	10.34 (-0.27)	10.29
MgO	37.99	40.80 (-0.35)	42.63 (+0.66)	44.71
CaO	3.33	2.64 (±0.00)	2.37 (+0.07)	1.56
Na2O	0.34	0.05	0.02	0.01
K2O	0.143	0.090	0.093	0.100
Cr2O3	0.29	0.30	0.30	0.29
total	100.00	100.00	100.00	100.00

adiabatic experiments

	PHN 1611	gel-4	gel-5	gel-6
SiO2	44.60	44.47 (+0.08)	44.02 (-0.11)	43.57
TiO2	0.26	0.16 (+0.02)	0.10 (+0.02)	0.05
Al2O3	2.81	1.96 (+0.09)	1.33 (+0.20)	0.72
FeO*	10.26	10.25 (-0.08)	10.16 (-0.13)	10.22
MgO	37.99	39.68 (-0.23)	41.46 (-0.17)	43.04
CaO	3.33	2.91 (+0.02)	2.49 (+0.11)	1.98
Na2O	0.34	0.19	0.06	0.01
K2O	0.143	0.096	0.084	0.100
Cr2O3	0.29	0.30	0.30	0.31
total	100.00	100.00	100.00	100.00

†; data from Nixon and Boyd (1973)
††; analyses of XRF except calculated values for Na2O and Cr2O3
†††; the differences from the calculated compositions

TABLE 10. Details of run conditions

isobaric experiments

Run #	P (kbar)	T (°C)	Duration (hr)	starting materials	Run products
459†	15	1275	36	PHN-1611	ol, opx, augite, gl
33	15	1350	71	gel-1	ol, opx, subcalsic augite, gl
34	15	1400	33	gel-2	ol, opx, subcalsic augite, gl
35	15	1425	29	gel-3	ol, pigionite, gl

adiabatic experiments

Run #	P (kbar)	T (°C)	Duration (hr)	starting materials	Residue
465†	20	1350	30	PHN-1611	ol, opx, cpx, gl
36	15	1311(-2)††	23	gel-4	ol, opx, cpx, gl
37	10	1276	77	gel-5	ol, opx, cpx, gl
38	5	1240(-4)††	44	gel-6	ol, opx, cpx (no glass)
39	0.001	1235	45	gel-6	ol, opx, cpx, sp, gl
40	5	1240(+5)††	44	PHN-1611	ol, opx, cpx, gl

†; data from Kushiro (1993)
††; the differences from the calculated values

TABLE 11. Compositions of incremental liquid

isobaric incremental batch melting

Run#	459†	33	34	35
P (kbar)	15	15	15	15
T (°C)	1275	1350	1400	1425
starting material	PHN-1611	gel-1	gel-2	gel-3
SiO2	49.65	49.27	50.64	52.03
TiO2	1.65	1.57	0.60	0.69
Al2O3	17.74	13.68	7.78	4.37
FeO*	7.80	9.04	10.82	11.49
MgO	8.85	11.94	15.67	16.60
CaO	9.54	11.20	12.57	11.32
Na2O	2.93	0.89	0.19	0.36
K2O	1.43	2.30	1.28	2.72
Cr2O3	0.12	0.12	0.46	0.42
Total	99.71	100.00	100.00	100.00
Fo mole %	87.3	88.5	88.7	88.3
Kd (Fe/Mg)	0.294	0.306	0.329	0.341
F††	0.098	0.039	0.073	0.037
incremental F	0.098	0.035	0.063	0.030
accumulated F	0.098	0.133	0.196	0.226

batch melting†

P (kbar)	15	15	15	15
T (°C)	1275	1300	1325	1350
SiO2	49.65	48.68	49.88	49.03
TiO2	1.65	1.29	1.20	1.23
Al2O3	17.74	16.20	14.21	14.32
FeO*	7.80	8.61	9.05	9.27
MgO	8.85	10.84	11.55	12.03
CaO	9.54	11.05	11.23	11.23
Na2O	2.93	1.98	1.70	1.69
K2O	1.43	0.84	0.76	0.69
Cr2O3	0.12	0.19	0.20	0.27
Total	99.71	99.68	99.78	99.76
F††	0.098	0.167	0.184	0.203

batch melting†

P (kbar)	15	15	15
T (°C)	1400	1425	1450
SiO2	50.31	50.26	51.27
TiO2	0.89	0.72	0.66
Al2O3	11.18	10.23	9.22
FeO*	9.86	10.02	10.40
MgO	14.57	16.81	17.33
CaO	10.88	9.60	9.15
Na2O	1.30	1.20	0.96
K2O	0.52	0.39	0.37
Cr2O3	0.35	0.51	0.43
Total	99.86	99.74	99.79
F††	0.269	0.359	0.378

†; data from Kushiro (1993)

††; degree of partial calculated from K2O abundance

TABLE 12. Compositions of incremental melt, accumulated melt and batch melt formed in the decompressional experiment

decompressional incremental batch melting

incremental melt

Run#	465†	36	37
P (kbar)	20	15	10
T (°C)	1350	1311(-2)††	1276
starting material	PHN-1611	gel-4	gel-5
SiO2	47.50	49.38	51.51
TiO2	1.91	1.29	1.05
Al2O3	16.36	13.83	12.59
FeO*	9.24	9.65	8.94
MgO	10.43	11.55	11.20
CaO	9.55	10.53	12.01
Na2O	2.49	2.12	0.95
K2O	2.18	1.48	1.65
Cr2O3	0.09	0.17	0.10
Total	99.75	100.00	100.00
Fo mole %	87.4	87.7	88.1
Kd (Fe/Mg)	0.290	0.299	0.302
F†††	0.064	0.065	0.051

accumulated melt

P (kbar)	20	15	10	5
T (°C)	1350	1311(-2)††	1276	1240(-4)
starting material	PHN-1611	gel-4	gel-5	gel-6
SiO2	47.50	48.47	49.26	49.26
TiO2	1.91	1.61	1.47	1.47
Al2O3	16.36	15.16	14.49	14.49
FeO*	9.24	9.45	9.32	9.32
MgO	10.43	10.99	11.04	11.04
CaO	9.55	10.04	10.55	10.55
Na2O	2.49	2.31	1.96	1.96
K2O	2.18	1.84	1.79	1.79
Cr2O3	0.09	0.13	0.12	0.12
Total	99.75	100.00	100.00	100.00
incremental F	0.064	0.061	0.044	0.000
accumulated F	0.064	0.125	0.169	0.169

batch melting

P (kbar)	20	15	10	5
T (°C)	1350	1311††††	1276††††	1240
SiO2	47.50	49.21	51.00	52.32
TiO2	1.91	1.25	1.07	1.10
Al2O3	16.36	15.32	15.08	15.50
FeO*	9.24	8.80	7.90	7.33
MgO	10.43	11.15	10.57	9.28
CaO	9.55	11.13	11.60	11.67
Na2O	2.49	1.86	1.62	1.74
K2O	2.18	0.80	0.65	0.66
Cr2O3	0.09	0.18	0.22	0.27
Total	99.75	99.71	99.71	99.87
F†††	0.064	0.174	0.215	0.212

†; data from Kushiro (1993)
††; the differences from the calculated values
†††; degree of partial melting calculated from K2O abundance
††††; estimated from Kushiro (1993)

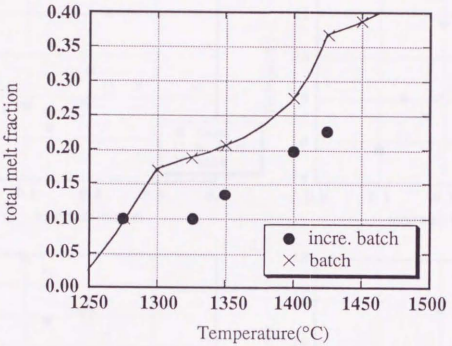

Fig. 15. Change of total melt fractions formed by incremental batch melting and by batch melting with increasing temperature at 15 kbar. Data of batch melting process are from Kushiro (1993).

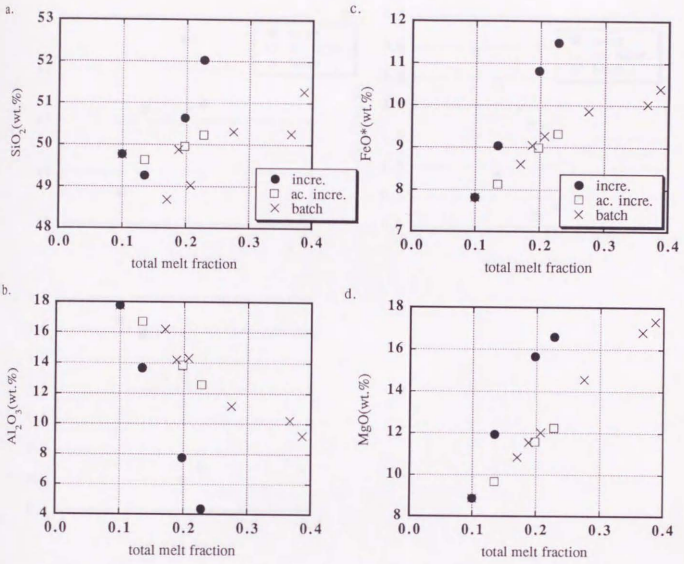

Fig. 16. Compositional change of incremental melts, accumulated incremental melts and batch melts with increasing melt fraction formed at 15 kbar. (a) SiO_2, (b) Al_2O_3, (c) FeO*, (d) MgO, (e) CaO, (f) TiO_2 and (g) Na_2O contents. Note that accumulated incremental melts are similar in composition to batch melts with the same melt fractions.

e.

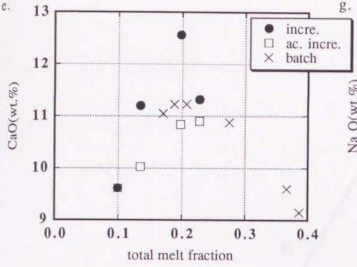
13
12
11
10
9
CaO(wt.%)
0.0
0.1
0.2
0.3
0.4
total melt fraction
incre.
ac. incre.
batch

g.

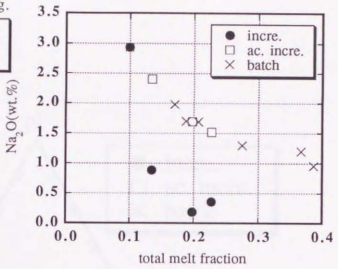
3.5
3.0
2.5
2.0
1.5
1.0
0.5
0.0
Na_2O(wt.%)
0.0
0.1
0.2
0.3
0.4
total melt fraction
incre.
ac. incre.
batch

f.

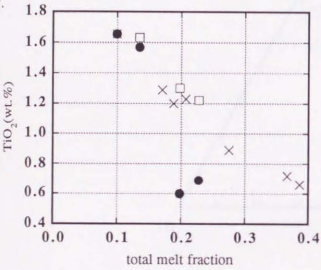
1.8
1.6
1.4
1.2
1.0
0.8
0.6
0.4
TiO_2(wt.%)
0.0
0.1
0.2
0.3
0.4
total melt fraction

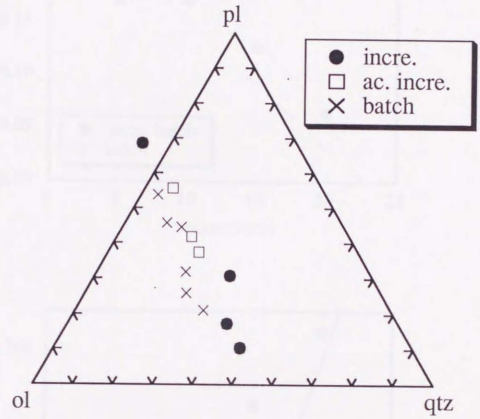

Fig. 17. Normative compositions of incremental melts, accumulated incremental melts and batch melts plotted on the Walker's ternary diagram olivine-plagioclase-quartz (Walker et al., 1979).

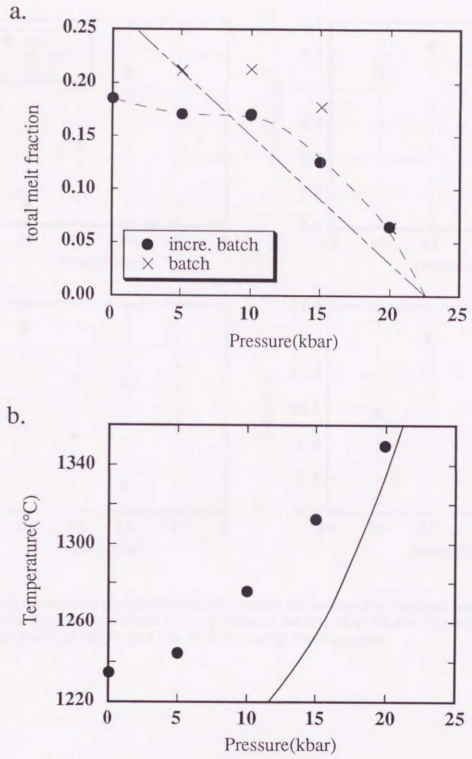

Fig. 18. (a) Accumulated incremental melt fractions and batch melt fractions formed by step-wise adiabatic decompressional melting of peridotite. A point and broken line shows the melt production rate 1.2 %/kbar used in the modelling by Klein and Langmuir (1987). It is notable the rate of melt production decrease from 22.5 kbar to lower pressures. (b) The change of temperature of peridotite generating melt by incremental batch melting. Solid line shows the dry solidus of PHN-1611 (Kushiro, 1993).

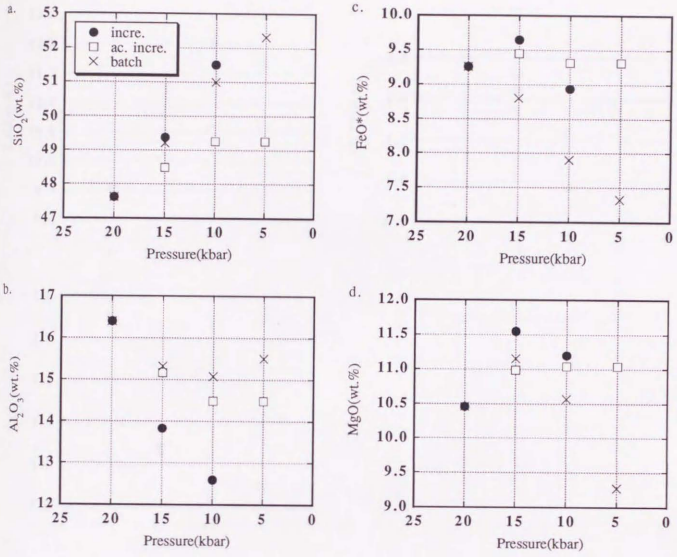

Fig. 19. Compositional change of incremental melts, accumulated incremental melts and batch melts formed by adiabatic decompressional melting of peridotite. (a) SiO_2, (b) Al_2O_3, (c) FeO*, (d) MgO, (e) CaO, (f) TiO_2 and (g) Na_2O contents.

e.

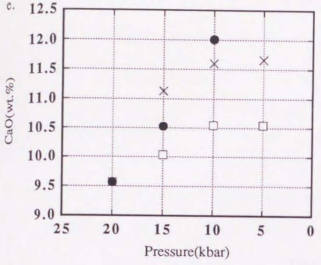
12.5
12.0
11.5
11.0
10.5
10.0
9.5
9.0
CaO(wt.%)
25 20 15 10 5 0
Pressure(kbar)

f.

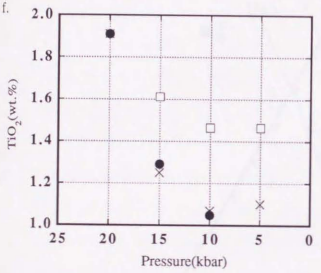
2.0
1.8
1.6
1.4
1.2
1.0
TiO2(wt.%)
25 20 15 10 5 0
Pressure(kbar)

g.

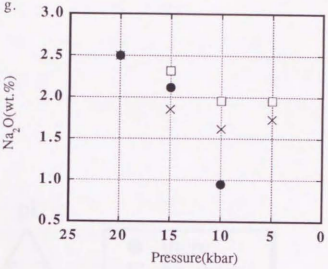
3.0
2.5
2.0
1.5
1.0
0.5
Na2O(wt.%)
25 20 15 10 5 0
Pressure(kbar)

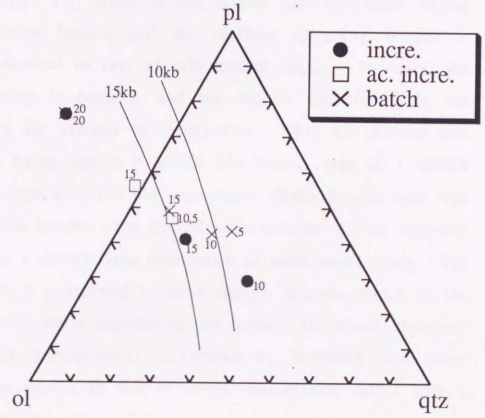

Fig. 20. Normative compositions of incremental melts, accumulated incremental melts and batch melts formed by step-wise adiabatic decompressional melting of peridotite are plotted on the Walker's ternary diagram olivine-plagioclase-quartz (Walker et al., 1979). The isobaric univariant curve for batch melts are shown for comparison (Kushiro, 1993).

V. Petrology and Evolution of the Central Ridge in North Fiji Basin; A Case Study of Ridge Magmatism

ABSTRACT

The North Fiji Basin is the largest back-arc basin among presently active basins, and the seafloor spreading feature is regionally identical to that of mid-oceanic ridges. However, the tectonic setting is complex and the basalts collected from the Central ridge are variable in composition. They are divided into four magma types; type I: N-MORB like basalts, type II: E-MORB like basalts, type III: OIB like transitional alkalic basalts, and type IV: BABB like basalts. The Central ridge consists of four segments and each has a characteristic distribution of these basalt types. The N-S segment is considered to be a mature segment which is the oldest and most active segment in this basin. The basalt chemistry are relatively homogeneous resembling to N-MORB and ridge topography is similar to that of normal mid-oceanic ridges with a medium spreading rate. The relatively long distance more than 300 km from the trench and the temporal evolution within 10 million years result in a seafloor spreading in back-arc basin similar to that at normal mid-oceanic ridges. In contrast, the N160 segment is in a stage of crustal extension rather than seafloor spreading. Collected glasses show a marked compositional variation and the geochemically enriched basalts are dominant. In 170E segment which is relatively close to the trench about 150 km in distance, the compositions of basalts are also widely ranged including type IV basalts like typical BABB. It suggests that the

genetic influence of the supra-subduction zone mantle is restricted to the area close to the convergent margin. Type III and IV basalts have higher H_2O contents than type I and II basalts and distinct major element compositions from them, showing that they were formed at significantly lower temperatures. He isotope ratios are generally higher ($^3He/^4He$ 7.2-10.7 R/R_A) than the mean MORB values, showing that the dominant source mantle for the North Fiji Basin basalts includes slightly primitive mantle component.

V-1. Introduction and geological setting

The North Fiji Basin is the largest and oldest active marginal basin in the southwestern Pacific, which has been formed since at least 8-10 Ma (Fig. 21) (Malahoff et al., 1982; Auzende et al., 1988; Charvis and Pelletier, 1989). This long-lived basin regionally shows the seafloor spreading similar to that of normal oceanic ridges. However, the North Fiji Basin has a complex history in its formation, and several ridge jumps are recognized (Tanahashi et al., 1991; Auzende et al., 1991). The crust of the North Fiji Basin is being formed dominantly along the Central ridge, although magmatism is also recognized in other area such as the South Pandora ridge and the Fiji Fracture Zone (Fig. 21) (Sinton et al., 1988; Johnson and Sinton, 1990). The Central ridge would have been formed at about 3 Ma (Auzende et al., 1988) and is presently propagating northward, suggesting that the northern part would be an incipient ridge.

The Central ridge consists of four segments; N160 segment, N15 segment, N-S segment and 170E segment (Fig. 22). The N160

segment is topographically distinctive from other segments and is composed of short echelon grabens with axial valley about 3500-4000 m deep (Fig. 24). It is probably in a stage of crustal extension rather than seafloor spreading, and the comparison with other segments would suggest the temporal evolution of the back-arc opening. In contrast, south of the 17°S triple junction, the depth is relatively shallow and constant about 2500 m. The axial high is recognized at the N15 and N-S segments suggesting a relatively active volcanic activities (Tanahashi et al., 1991). The N-S segment is the oldest and the relatively most active segment with the fastest spreading rate of about 8 cm/y and a morphology very similar to that of East Pacific Rise.

The Central ridge is associated with the New Hebrides Trench, which trends from NNW to SSE and is located 500~150 km west of the ridge. The role of fluid dehydrated from the slab is suggested to be important for the genesis of back-arc basin basalts (e.g. Hawkins and Melchior, 1985; Sinton and Fryer, 1987; Falloon et al., 1992; Hawkins et al., 1990; Saunders and Tarney, 1984), and its genetic influence probably changes with increasing distance from the convergent margin. The most active N-S segment is located about 300 km east of the trench that is characteristically far away compared to the smaller back-arc basins such as the Mariana Trough and the Lau Basin. The 170E segment is relatively close to the convergent margin located about 150 km from the trench, so that the influence of fluid can be more significant (Fig. 21).

The Central ridge was surveyed during the STARMER project (France and Japan cooperative study) during the cruises of *R/V Kaiyo* and *Yokosuka* from 1987 to 1991. This project includes the comprehensive sea-beam mapping and detailed sampling from the

whole Central ridge by dredging and *Nautile* and *Shinkai6500* at 19 stations from 15°58'S to 21°24'S (Table 13; Fig. 22). The collected basalts have a f compositional range and their distribution characterizes the magma generation at each segment. We present major and minor elements and He isotope of these samples with reference to the trace element and isotope compositions from separate paper (Nohara et al., 1993), and discuss about their petrogenesis and the back-arc basin magmatism.

V-2. Chemistry of samples

Most samples are fragments of pillow or sheet lavas with the fresh glass margins that are expected to be nearly zero-age except dolerites were collected from station 56. Most are aphyric to moderately phyric (with less than 15% phenocrysts) with exception of plagioclase porphyritic rocks from stations 5 and 17. Basalts with both olivine and plagioclase phenocrysts are common, but clinopyroxene phenocrysts are also present in basalts from several stations.

We analyzed 270 glass chips from 70 samples and minerals by electron microprobe JEOL 733 Mk.II at *Geological Institute, University of Tokyo*. Bulk chemistry was determined for a subset of these samples for minor elements by XRF Phillips PW1480 at *Geological Survey of Japan*. Fresh glasses from 7 samples were processed for He isotope analysis at *Department of Earth and Planetary Physics, University of Tokyo*. Analytical procedures for He isotope were described elsewhere (Hiyagon et al., 1992).

2.1. Major and minor elements

Glass compositions range from basalt to basaltic andesite (SiO_2 48-53 wt.%, Mg# 47-69) (Table 14) and show wide range in K_2O content from 0.04 to 1.36 wt.%. The most common samples are K-depleted basalts (< 0.2 wt% K_2O) which are quite similar to N-MORB in major, trace and isotope compositions. Enriched basalts, however, resembling to E-MORB and oceanic island basalts (OIB) are dominant in N160 segment, and we also collected glasses similar in major and minor elements to back-arc basin basalts (BABB) described by Sinton and Fryer (1987) at the Mariana Trough at one locality close to the trench.

The North Fiji Basin glasses are divided into four magma types based on K_2O contents (Fig. 23) and this classification well correlates with other major and trace element characteristics. Figure 25 shows their major element chemistry comparing with the representative N-MORB glasses from the East Pacific Rise and BABB glasses from the Mariana Trough (Hawkins et al., 1990; Allan et al., 1989; Michael and Chase, 1987). Figure 26 shows the trace element abundances normalized to N-MORB of each basalt type.

Type I basalts - They are characterized by low K_2O content, and their major element chemistry is similar to that of typical N-MORB (Fig. 25). The type I basalts form a single liquid line of descent with some scattering ranging from 6.2 to 9.4 wt.% MgO. The spider-diagram (Fig. 26) also shows their similarity to N-MORB, except they are slightly enriched in Rb and Ba and some samples are comparative to the type II basalts in these elements. The little depletion in Nb is clearly displayed and the enrichment in Sr is also observed in some samples, although they are less significant than

the Mariana Trough basalts (e.g. Hawkins et al., 1990). REE data show depleted to flat chondrite-normalized patterns, and Sr and Nd isotope data are within the range of N-MORB (Nohara et al., 1993). The type I basalts are most widely and commonly collected from all the segments and probably are the representative of the crust presently being formed in the North Fiji Basin.

Type II basalts - They are geochemically enriched type of basalts and figure 26 shows they have strong affinity to E-MORB with significant enrichment in large ion lithophile elements (LILE), light rare earth element (LREE) relative to type I basalts. They have generally similar Nd and Sr isotope compositions to the type I basalts, but some are also enriched in these compositions (Fig. 24). Figure 25 shows that the type II basalts are generally similar in major element compositions to type I basalts, but they have slightly higher Al_2O_3 and lower FeO* contents. Samples from station 21 are chemically distinctive with significantly lower CaO and higher Na_2O and TiO_2 contents. Type II basalts are close to BABB in LILE and LREE, but do not share the Al, Fe and high field strength elements (HFSE) characteristics. Basalts of this type are common in the N160 segment and were also collected at near the edge of the segment (Fig. 24).

Type III basalts - They are K-enriched transitional alkalic basalts (up to 0.6% norm Ne). They have distinct major element compositions from type I basalts with significantly high Al_2O_3 and TiO_2 and low FeO and CaO contents, which are within the range of BABB but distintive in TiO_2 content (Fig. 25). The spider-diagram (Fig. 26) shows their similarlity to OIB with significant enrichment in LILE (K_2O 0.7-1.4 wt.%) and LREE compared to N-MORB, and they also enriched in Sr and Nd isotope compositions. The type III

basalts appear only in the north of the triple junction in the Central ridge, and those with similar trace element characteristics were also recovered at the South Pandora ridge in the northern part of the North Fiji Basin and at the Fiji Fracture zone (Sinton et al., 1988; Johnson and Sinton, 1990; Eissen et al., 1993).

Type IV basalts - They are characterized by depletion of HFSE (clearly in Nb) and enrichment of LILE (including Sr) and LREE, and have major element compositions sharing the characteristics with BABB collected in the Mariana Trough (Figs. 25 and 26) (e.g. Hawkins and Melchior, 1985; Sinton and Fryer, 1987). Nd and Sr isotope compositions, however, are close to the associated type I basalts (Fig. 24). All were evolved basaltic andesites, but have compositional similarlity with the type III basalts except low HFSE contents relative to them. The type IV basalts were collected only from the station 23 in the 170E segment which is a closest segment to the convergent margin.

2.2. He isotope

$^3He/^4He$ ratios were determined for 7 samples of the type I basalts from the N15 and N-S segments and the type II and III basalts from the N160 segment as shown in Table 15 and Fig. 28. The analyses are generally higher values than the mean MORB values ($R/R_A \approx 8$) ranging from 7.19 to 10.72 times atmospheric ratio. It shows that the dominant source mantle for the North Fiji Basin basalts includes a slightly primitive undegassed mantle component. Figure 29 displays the He isotope data versus K/Ti ratios, showing that the geochemically enriched type II and III basalts have comparative or less He isotope compositions than the

depleted type I basalts. Two samples (ST55-D11-1-6 and ST58-DT8/9-7) have relatively low He isotope ratios; however, they have significantly low ^{4}He concetrations, suggesting that it might be due to the effects of gas loss and crystallization.

V-3. Along axis variations

N160 segment and triple junction area - The N160 segment has a deep axial valley mostly covered with sediments, suggesting that volcanic activity has been relatively most inactive in the Central ridge. Collected basalts are most variable in composition which consist of three magma types with a wide range in Nd isotope and trace element compositions. The geochemically enriched type II and III basalts are dominant in this area, but depleted type I basalts are also associated with them sometimes at the same stations. Two different types of basalts were recovered from the adjacent localities at station 4 and 58 or in the single dredge haul at station 55, showing that the source mantle is locally very heterogeneous. The marked compositional variation in MgO content shows that melts were evolved by the variable degree of differentiation (Fig. 24).

N15 and N-S segments - In these two segments, the ridge has an axial high and the sedimentary sequence cannot be identified on the seismic profiles near the axial area (< 50 km from the axis) (Tanahashi et al., 1991). Basalts mostly are N-MORB like type I basalts, although type II basalts were also collected from near the edge of the N15 segment. The source mantle is relatively

homogeneous resembling to a N-MORB source mantle with slight enrichment in Rb and Ba and depletion in Nb displayed in Fig. 26.

170E segment - This segment is located at the southern end of the Central ridge and is relatively close to the trench about 150 km in distance. Glasses show a marked compositional variation in terms of both major and minor elements with variable H_2O content consisting of N-MORB, E-MORB and BABB like basalts, reflecting the heterogeneity in the source mantle although Nd isotope ratios are homogeneous (Fig. 24). Such local association of different types of basalts was also recognized in other back-arc basin such as Mariana Trough (Hawkins et al., 1990). Type I basalts are relatively abundant, and type II basalts with a distinct major element compositions from those in other segments were found at near the edge of the segment. BABB like type IV basalts were characteristically recovered from this segment. The depletion in Nb is observed in some type I basalts as well as type IV basalts (Fig. 26).

V-4. Petrogenesis

The four magma types found in the Cetnral ridge of the North Fiji Basin are widely ranged in chemical compositions, suggesting that they were formed under different conditions by partial melting of a heterogeneous source mantle and evolution at shallower depths. The higher amounts of water in enriched types of the North Fiji Basin basalt must have caused the different conditions of both magma generation and evolution from the

depleted basalts. Aggrey et al. (1988) and Danyushevsky et al. (1993) reported the high water abundances in the type II and III basalts from the N160 segment and the South Pandra ridge. Type I samples in the present classification have 0.21-0.33 wt.% H_2O, whereas a type II sample has 0.47% and type III samples have 0.74-1.54% H_2O. The water abundances in type IV basalts are unknown but probably similar to the type III basalts as discussed below.

Type I basalts are strikingly similar in composition to N-MORB and their major elements are plotted close to the field of typical N-MORB (Fig. 25). They form a single liquid line of descent that can be generally explained by fractional crystallization of olivine + plagioclase ± clinopyroxene (Eissen et al., 1991). On the other hand, the type III and IV basalts are similar to BABB in terms of major element, although the type III basalts are clearly different in TiO_2. The type III basalts form a separate liquid line of descent not pararell to that of type I basalts in figure 25. The compositions of type I, III and IV basalts are poltted on the ternary diagram olivine-plagioclase-silica (Fig. 27). It shows that they lie on the respective cotectic line but type III and IV basalts are displaced to the plagioclase apex compared to the type I basalts. This can be caused by the higher abundances of water in the type III and IV magmas, which expands the liquidus volume of olivine and clinopyroxene at the expense of plagioclase and suppresses plagioclase crystallization (Sinton and Fryer, 1987). The fact that all of the basalts with only olivine phenocrysts are type II and III basalts also indicates that water have played a role in their evolution.

The different trends between the type I and III basalts are clearly displayed in Al_2O_3, FeO*, CaO and TiO_2 contents. The differences in Al_2O_3 and FeO* contents could be explained by the differences in H_2O content (Michael and Chase, 1987). However, this displacement is observed even in the primitive basalt suite (Mg# >65), if not primary melts, which can be in equilibrium with mantle olivine (Fo 88-89) assuming Fe^{3+}/Fe^{2+} is 0.15 (Hawkins et al., 1990). Their respective parental magma compositions, therefore, are probably different in Al_2O_3 and FeO* contents.

The parental melt compositions of type I and III basalts are proposed in Table 16. Both liquid lines of decent are relatively not scattered (Fig. 25), and therefore they could be representatives of their respective parental suites. Both most magnesian samples can be in equilibrium with Fo 89 olivine when $(Fe^{2+}/Mg)_{ol}/(Fe^{2+}/Mg)_{glass}$ is 0.3. This value would be a little low for the type I basalts, since the sample ST17-D1-1 contains a large crystal of Fo 90 olivine, which may represent an equilibrium composition with their parental melts. Therefore, a primary melt for the type I magmas are calculated by incrementally adding 0.5 wt.% equilibrium olivine compositions to get a suggested Fe^{2+}/Mg ratio. The Fe^{3+}/Fe^{2+} ratio (= 1.5) may be too high for type I basalts with lower H_2O abundances, so that their parental melt might be more magnesian.

The primary melts for the type I basalts are similar in composition to the magnesian Mid-Atlantic Ridge basalt (Table 16) and also similar to the melt formed at 10 kbar and 1300°C determined by high pressure melting experiments (session II). The type III parental melt is transitional alkalic basalts and have same SiO_2, lower FeO*, MgO and CaO and higher TiO_2, Al_2O_3 and Na_2O

contents than type I parental melt. It can be explained by the different degrees of partial melting at similar pressures based on the batch melting model (e.g. Hirose and Kushiro, 1993; Kushiro, 1993).

The type III basalts has significantly higher H_2O concentrations (0.74-1.54 wt.%) than the type I magma (~0.2 wt.%), which must influence the magma generation. The presence of H_2O lowers the solidus temperature of mantle peridotite and increases the degree of partial melting. The results of experiments on the hydrous partial melting of peridotite at 10 kbar (session III) show that the melt formed at 1200°C (13.7 % melting) under the presence of water (1.5 % H_2O in melt) is quite similar in composition to the anhydrous 1300°C melt (12.1 % melting). This can not be directly applied to the genesis of the type III magma, but it strongly supports that the type III parental magma was formed under the significantly lower temperature.

The compositions of BABB like type IV basalts are plotted close to the extension of liquid line of decent for type III basalts except TiO_2 (Fig. 25), and both have probably comparative H_2O content. It suggests that they possibly have similar parental magmas, and the type IV primary melt may be generated also at lower temperature than N-MORB like magmas similarly to the type III parental melt.

The type II basalts from the N160 segment have intermediate compositions of major and minor element and H_2O contents between the type I and III basalts. Price et al. (1990) discussed that the enriched basalts from the N160 segment are formed from a mixed source of a typical N-MORB source mantle and an enriched mantle. Further work by Nohara et al. (1993) and Eissen et al.

(1993) also supported their conclusion and showed that the variations in trace element and isotope compositions of the North Fiji Basin basalts can be generally explained by the binary mixing of a depleted N-MORB component and a OIB-like component.

V-5. Evolution of back-arc basin magmatism

The North Fiji Basin shows a variable spreading feature reflecting the complex tectonic settings (Fig. 21), but the homogeneous basalt chemistry and ridge topography similar to those at normal mid-oceanic ridges with a medium spreading rate are regionally recognized in the N-S segment. This segment is the oldest and most active segment considered to be a "mature" segment. The distance more than 300 km from the trench and the temporal evolution within 10 million years form the seafloor spreading in the back-arc basin quite similar to that at normal mid-oceanic ridges.

The back-arc basin magmas have been discussed to be derived from the supra-subduction zone mantle which has been modified by previous melting events and by addition of fluid dehydrated from the subducted slab (e.g. Hawkins and Melchior, 1985; Sinton and Fryer, 1987). They contain relatively large amounts of H_2O (up to 2 wt.%) (e.g. Muenow et al., 1990) compared to N-MORB (~0.2 wt.%), and they must significantly influence the genesis of back-arc basin basalts. Hawkins et al.(1990) showed that the parental magmas for the Mariana Trough basalts are similar to the primitive N-MORB in terms of major elements but they have 0.5-1.5 wt.% H_2O. As discussed in the previous session,

under the presence of such higher amounts of water the parental BABB melts can be formed from the supra-subduction zone mantle at significantly lower temperatures than the parental N-MORB melts. The North Fiji Basin, however, is a relatively large basin, and the dominant North Fiji Basin basalts resemble to N-MORB not to BABB. The typical BABB defined at the Mariana Trough were collected only in the 170E segment which is relatively close to the trench about 150 km in distance. It shows that the genetic influence of such supra-subduction zone mantle is restricted to the area close to the convergent margin (Fig. 26).

It is recently recognized that the early stage of back-arc rifting is due to crustal extension rather than seafloor spreading (Leg 135 Scientific Party, 1992; Tamaki et al., 1992). The N160 segment is presently propagating northward and would be in a stage of crustal extension, reflecting the local heterogeneity in source mantle and the characteristic distribution of the type III basalts. They are close in composition to the OIB like basalts, but He isotope data do not suggest they were originated from an undegassed primitive mantle (Table 15). The source region beneath the N160 segment is considered to be a depleted suboceanic mantle which has been affected prior geochemical enrichment by silicate veins related to the Samoan hot spot located about 1500 km east of the ridge (Johnson and Sinton, 1988; Farley et al., 1992). Such mantle still remains and reflects the magma generation in a stage of crustal extension, although it is different from the supra-subduction zone mantle in the North Fiji Basin that would result from the long distance from the trench about 500 km.

Table 13. Sampling Locations

Operation*	Station	Location	Depth(m)	Site
northern segment				
Y90-D12	ST 56	15°37.8'S 173°20.9'E	3459	eastern flank of the graben
Y90-D11	ST 55	15°58.5'S 173°23.4'E	2962	off-ridge seamount near the western edge of the graben
Y90-D10	ST 54	15°59.4'S 173°29.5'E	3607	talus in the axial graben
Y90-DT8/9	ST 58	16°17.8'S 173°34.0'E	3599	talus of the graben
Y91-DV88	ST 58	16°20.1'S 173°32.9'E	3054	axial graben
Y90-D9	ST 53	16°27.1S 173°31.1'E	3464	axial graben
K88-D6	ST 29	16°39.9'S 173°35.0'E	2580	ridge near the axis
triple junction area				
K87-D3	ST 5	16°53.6'S 173.54.4'E	2205	triple junction area
K88-D1	ST 17	16°47.5'S 173°49.1'E	2778	triple junction area
K87-D2 STARMER I,II-DV	ST 4	16°54.7'S 173°54.7'E	1979	triple junction area
N15E segment				
K87-D5	ST 8	17°09.5'S 173°52.3'E	2306	axial graben
K87-D6	ST 9	17°19.9'S 173°49.3'E	2506	small axial graben
K87-D9	ST 12	17°36.1'S 173°46.2'E	2517	axial ridge
K87-D4	ST 6	18°06.0'S 173°29.0'E	2816	axial ridge
K87-TV1	ST7	18°06.7'S 173°28.6'E	2696	axial ridge
N-S segment				
K87-D10	ST 14	18°49.5'S 173°29.8'E	2729	axial ridge
K87-D11	ST 15	19°17.1'S 173°27.3'E	2755	axial ridge
southern segment				
K88-D3	ST 21	21°02.2S 174°08.9'E	2844	axial ridge
K88-D4	ST 23	21°10.7'S 174°11.0'E	2834	axial ridge
K88-D5	ST 22	21°23.8'S 174°11.9'E	2653	axial ridge
K88-DT9/10	ST 22	21°26.7'S 174°10.7E	2218	axial ridge and seamount

*: Y; YOKOSUKA cruise, K; KAIYO cruise, D; dredge, DT; deep tow survey, TV; photo-video run, DV; dives

Table 14. Microprobe glass analyses and trace elements

sample No.	ST55-D11-1-6	ST55-D11-1-7	ST55-D11-2-5	ST54-D10-1	ST58-DT8/9-1	ST58-DT8/9-7	ST58-DV88-2	ST53-D9-1-3	ST53-D9-1-4	ST53-D9-2-1	ST29-D6-1	ST29-D6-3
SiO2	49.90	49.49	49.74	50.62	50.62	50.56	50.51	50.33	50.53	50.76	50.49	50.28
Al2O3	16.14	16.62	14.92	16.34	15.60	16.20	16.54	16.23	15.91	16.42	14.53	14.71
TiO2	1.67	1.17	1.64	2.49	1.46	2.59	1.97	1.42	1.37	1.23	1.86	1.98
FeO	9.01	8.62	10.32	8.80	9.07	8.02	7.98	7.98	7.86	8.48	10.24	10.85
MnO	0.10	0.16	0.23	0.20	0.17	0.15	0.01	0.08	0.18	0.19	0.13	0.27
MgO	8.00	9.21	8.07	6.40	8.14	6.43	7.22	8.68	8.27	8.34	6.85	7.15
CaO	11.51	12.26	11.37	9.90	11.94	10.14	10.83	11.73	12.21	11.99	11.86	11.55
Na2O	2.84	2.51	2.79	3.07	2.59	3.30	2.87	2.62	2.58	2.56	2.91	2.71
K2O	0.32	0.11	0.18	1.36	0.30	0.86	1.10	0.45	0.38	0.42	0.19	0.29
total	99.68	100.37	99.58	99.23	100.04	98.49	99.08	99.79	99.36	100.48	99.24	99.93
Mg#	0.613	0.656	0.582	0.564	0.615	0.588	0.617	0.660	0.652	0.637	0.544	0.540
type	II	I	I	III	II	III	III	II	II	II	I	I
Zr	126	76	96	214	96	175			84		112	107
Y	33	28	35	29	27	33			23		29	30
Sr	209	147	126	381	180	265			183		173	154
Rb	6	1	2	24	8	21			7		3	6
Ba	72	7	22	364	66	210			86		14	36
Nb	11		4.81	62.81	7.52	22.06	41.63		10.89		3.58	3.25
Ni	110	166	123	128	131	243			264		104	105
V	296	260	332	306	279	301			271			
Cr	333	368	260	288	325	426			664			

sample No.	ST29-D6-7	ST5-D3-1	ST17-D1-2	ST4-DV7-1	ST4-D2-5	ST4-D2-9	ST4-DV16-2	ST4-DV21-4	ST4-DV21-5	ST8-D5-1	ST8-D5-4	ST9-D6-2
SiO2	50.65	48.90	50.72	49.94	50.58	51.11	50.42	48.98	48.98	50.01	51.11	50.05
Al2O3	15.04	16.26	14.04	16.34	14.73	14.66	15.01	17.81	17.79	13.81	14.16	14.43
TiO2	1.85	0.98	1.36	1.00	1.52	1.60	1.39	1.86	1.87	1.79	1.78	1.46
FeO	9.55	8.00	11.00	8.94	10.16	10.41	9.38	7.36	7.22	11.82	11.66	10.79
MnO	0.11	0.19	0.22	0.10	0.24	0.29	0.24	0.12	0.21	0.14	0.18	0.24
MgO	7.32	9.23	7.33	9.18	7.77	7.48	7.81	7.75	8.39	6.49	6.81	7.40
CaO	11.54	12.40	11.91	12.88	11.96	11.80	12.01	11.08	10.97	11.06	11.08	11.86
Na2O	2.80	2.44	2.83	2.30	3.00	3.04	2.81	2.72	2.87	2.98	2.89	2.80
K2O	0.30	0.12	0.11	0.02	0.14	0.12	0.13	0.76	0.76	0.15	0.16	0.11
total	99.21	98.51	99.64	100.88	100.29	100.60	99.20	98.43	99.05	98.23	99.83	99.14
Mg#	0.577	0.673	0.543	0.647	0.577	0.561	0.597	0.652	0.674	0.495	0.510	0.550
type	I	I	I	I	I	I	I	III	III	I	I	I
Zr					93	85				91	91	84
Y					28	28				31	31	28
Sr					143	127				114	113	117
Rb					2	2				3	3	2
Ba					18	29				35	27	29
Nb					2.69	2.51			22.95	2.87	3.54	3.75
Ni					67	60		175	181	76	61	61
V								236	243			111
Cr								278	283			

Table 14 (continued)

sample No.	ST9-D6-3	ST9-D6-6	ST12-D9-9	ST6-D4-3	ST6-D4-4	ST7-DT1-3	ST14-D10-1	ST14-D10-4	ST14-DT7-2	ST14-N17-5	ST15-D11-1
SiO2	49.55	50.40	50.09	50.74	51.00	50.66	49.89	50.29	49.40	50.71	49.45
Al2O3	14.40	13.64	15.97	14.55	14.82	16.10	14.68	14.88	15.42	13.82	14.90
TiO2	1.47	1.97	1.22	1.50	1.43	1.26	1.48	1.64	1.26	1.80	1.73
FeO	10.09	11.91	9.26	10.81	9.76	9.26	10.88	11.23	10.26	11.92	10.63
MnO	0.18	0.24	0.15	0.24	0.13	0.11	0.24	0.24	0.21	0.11	0.22
MgO	7.31	6.18	8.37	7.27	8.06	7.67	8.02	7.51	8.60	7.51	8.03
CaO	12.26	10.60	12.18	11.65	11.95	10.99	11.50	11.39	12.08	11.09	11.32
Na2O	2.83	3.04	2.52	3.11	2.46	2.79	2.45	2.80	2.40	2.55	2.72
K2O	0.12	0.20	0.11	0.13	0.03	0.43	0.10	0.22	0.07	0.10	0.15
total	98.21	98.18	99.88	99.99	99.63	99.27	99.24	100.18	99.68	99.62	99.14
Mg#	0.563	0.480	0.617	0.545	0.595	0.596	0.568	0.544	0.599	0.529	0.574
type	I	I	I	I	I	II	I	I	I	I	I
Zr	76			72			73	91	63		105
Y	25			27			29	29	25		32
Sr	123			95			85	140	81		119
Rb	1			1			1	3	1		2
Ba	18			11			15	35	15		10
Nb	2.45						1.83	3.86			2.6
Ni	65			107			111	88	117		104
V	110			117			71				
Cr											

sample No.	ST15-D11-12	ST21-D3-3	ST21-D3-9	ST23-D4-1	ST22-D5-1	ST22-DT9/10-1
SiO2	49.24	49.16	50.04	50.92	53.09	51.16
Al2O3	15.25	16.20	16.67	14.61	15.53	14.86
TiO2	1.78	2.12	1.81	1.38	1.12	1.57
FeO	10.84	9.12	8.50	10.28	9.83	10.58
MnO	0.17	0.20	0.11	0.32	0.16	0.16
MgO	7.82	8.51	8.22	7.86	5.39	7.17
CaO	11.50	10.18	10.60	11.96	9.89	11.06
Na2O	2.84	3.00	3.06	2.68	3.37	2.84
K2O	0.15	0.46	0.40	0.06	0.42	0.13
total	99.59	98.96	99.42	100.06	98.80	99.52
Mg#	0.562	0.624	0.633	0.577	0.494	0.547
type	I	II	II	I	IV	I
Zr	110	160	130	69	79.9	100
Y	37	37	32	26	25.5	36
Sr	121	245	237	104	336	136
Rb	2	5.76	5.98	2	6.1	2
Ba	6	70	64	12	63.8	19
Nb			7.9	1.28	1.51	
Ni	119	197	215	71	29.5	69
V						179
Cr		311	340			

Table 15. Helium isotope ratios in North Fiji Basin basalts

sample	type	3He/4He (R/RA)	4He (10-6 ccSTP/g)
ST55-D11-1-6	II	8.37±1.43	0.51
ST58-DT8/9-7	III	7.19±0.82	0.29
		8.22±0.76	0.76
ST53-D9-1-3	II	10.72±0.68	2.33
ST4-D2-1	I	10.01±0.54	12.0
ST6-D4-4	I	9.34±1.84	5.44
ST14-DT7-2	I	9.41±0.57	11.6
ST15-D11-1	I	9.91±0.68	12.0

Table 16. Compositions of representative primary melts for type I and III basalts, a magnesian MORB 519-4-2 (Bryan amd Moore, 1977) and batch melt at 10 kbar

	type I	type III	519-4-2	10kbar melt(run #2)
SiO2	49.34	49.45	49.38	49.59
TiO2	0.96	1.89	0.74	0.79
Al2O3	15.94	17.96	16.32	16.49
FeO*	8.20	7.29	8.99	8.89
MnO	0.18	0.21	0.16	0.12
MgO	10.72	8.47	10.44	10.35
CaO	12.15	11.08	11.69	11.27
Na2O	2.39	2.90	2.17	2.15
K2O	0.11	0.77	0.07	0.15
Total	100.00	100.01	99.96	99.81

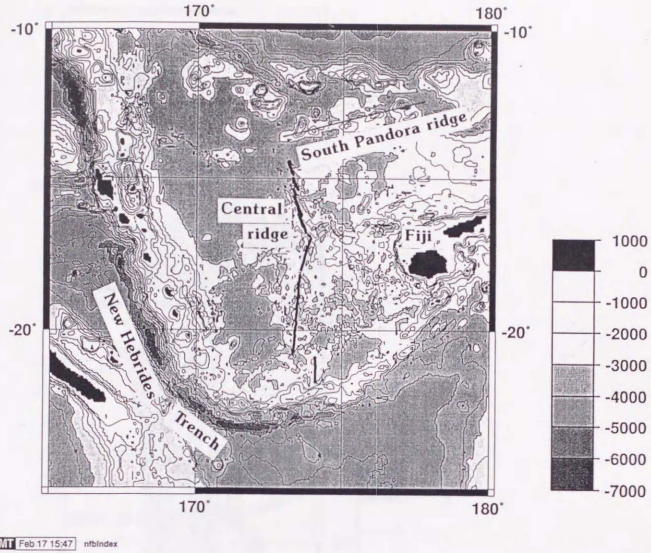

Fig. 21. Map of the North Fiji Basin. The solid lines show the ridge axis of the Central ridge.

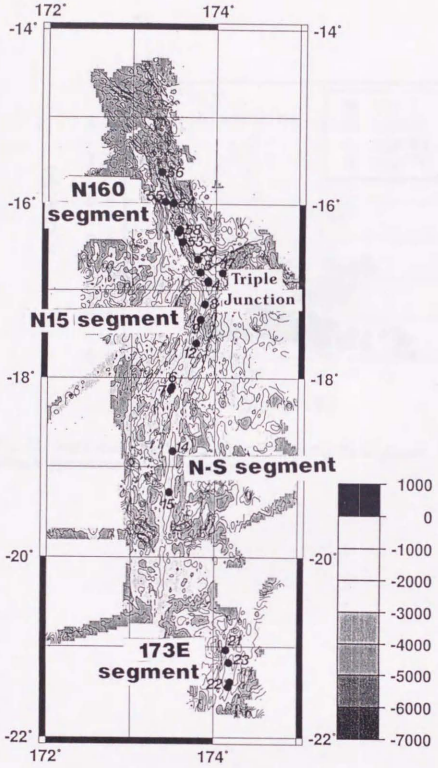

Fig. 22. Sampling locations. The Central ridge consists of four segments; N160 segment, N15 segment, N-S segment and 170E segment from north to south.

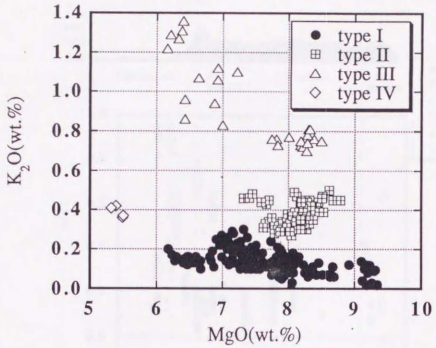

Fig. 23. MgO versus K_2O (wt.%) for the North Fiji Basin glasses. The classifications of each type are based on this diagram.

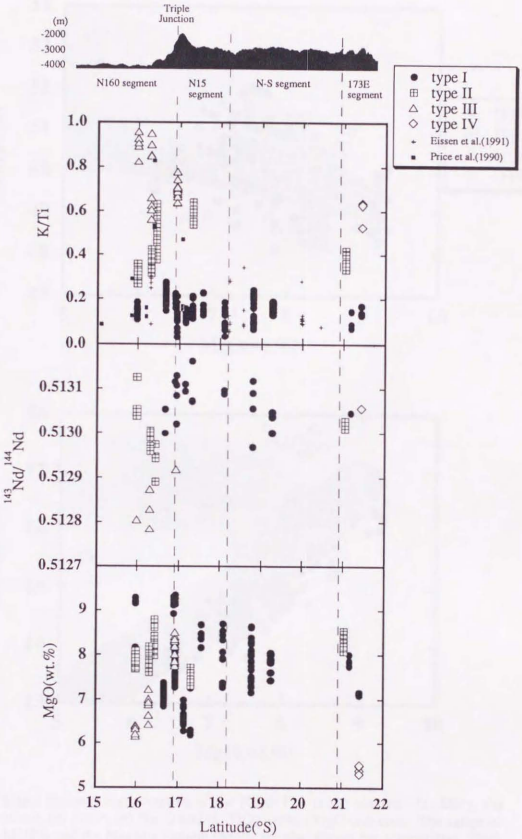

Fig. 24. Variation of axial water depth and basalt chemistry along the axis. Nd isotope data are from Nohara et al. (1993).

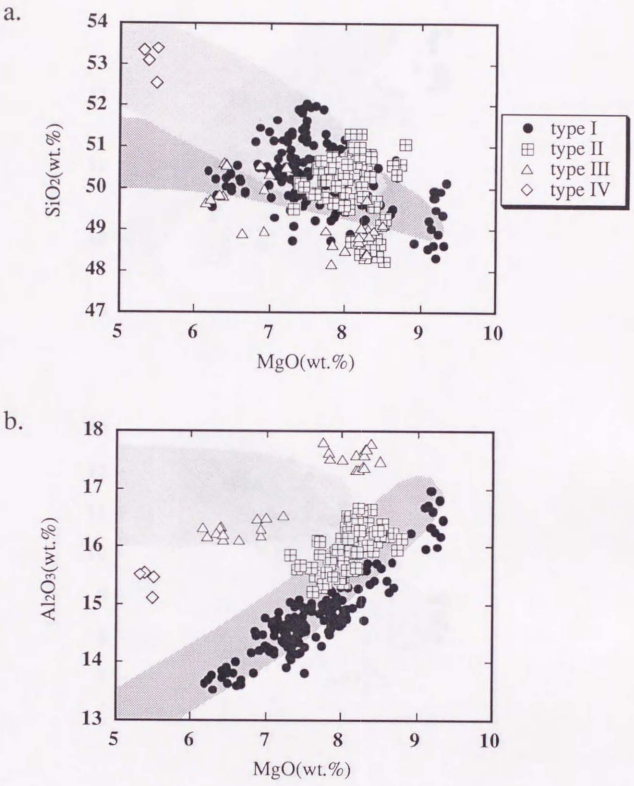

Fig. 25. Major element compositions of the North Fiji Basin glasses. (a) SiO_2, (b) Al_2O_3, (c)CaO, (d) FeO*, (e) Na_2O and (f) TiO_2 versus MgO contents. The range of typical N-MORB and the Mariana Trough basalts are also shown for comparison. Dark stippled area: N-MORB suite (Allan et al., 1989; Michael and Chase, 1987); Light stippled area: Mariana Trough basalts suite (Hawkins et al., 1990).

c.

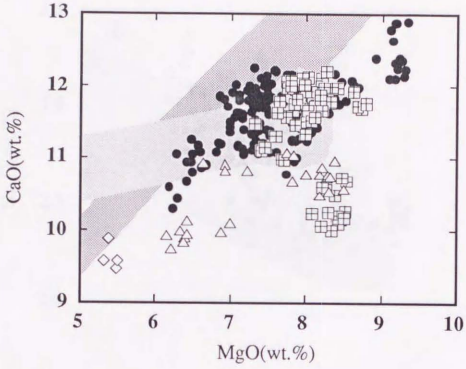
13
12
11
10
9
CaO(wt.%)
5
6
7
8
9
10
MgO(wt.%)

d.

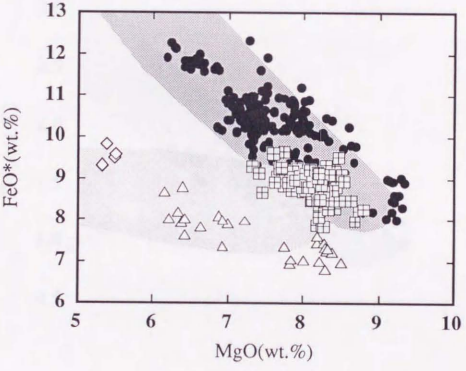
13
12
11
10
9
8
7
6
FeO*(wt.%)
5
6
7
8
9
10
MgO(wt.%)

e.

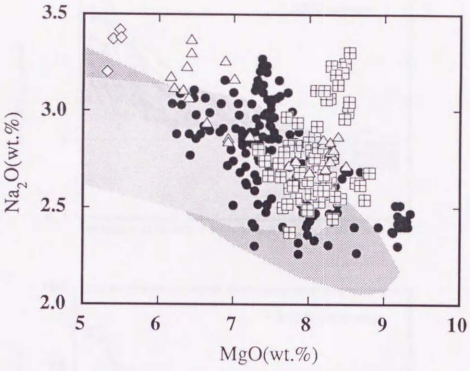
3.5
3.0
2.5
2.0
Na_2O(wt.%)
5
6
7
8
9
10
MgO(wt.%)

f.

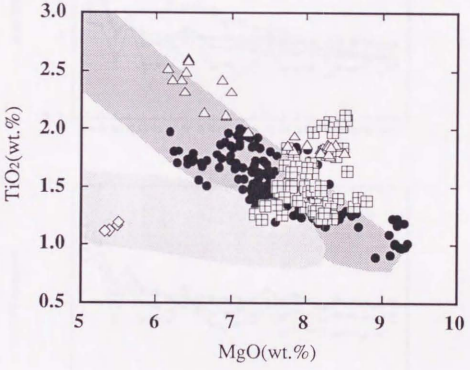
3.0
2.5
2.0
1.5
1.0
0.5
TiO_2(wt.%)
5
6
7
8
9
10
MgO(wt.%)

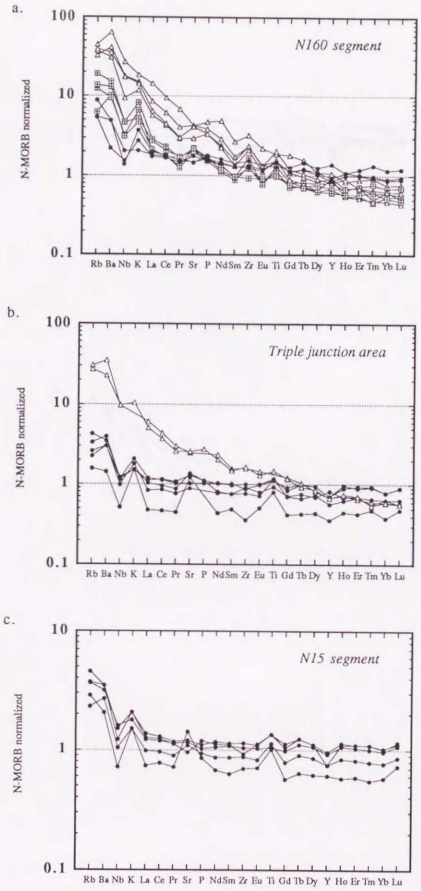

Fig. 26. Trace element abundances for selected basalts of each segment normalized to N-MORB (Sun and McDonough, 1989). (a) N160 segment, (b) triple junction area, (c) N15 segment, (d) N-S segment and (e) 170E segment. Symboles showing each basalt type are same with those in the previous diagrams. Data are from Nohara et al. (1993).

d.

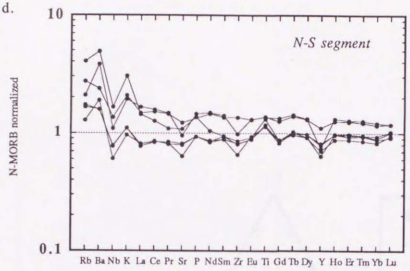
N-S segment
N-MORB normalized
10
1
0.1
Rb Ba Nb K La Ce Pr Sr P NdSm Zr Eu Ti Gd Tb Dy Y Ho Er Tm Yb Lu

e.

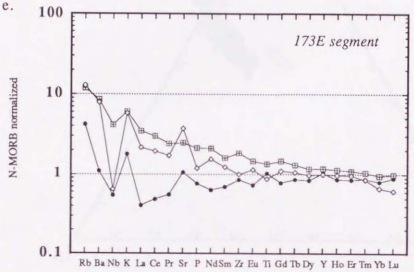
173E segment
N-MORB normalized
100
10
1
0.1
Rb Ba Nb K La Ce Pr Sr P NdSm Zr Eu Ti Gd Tb Dy Y Ho Er Tm Yb Lu

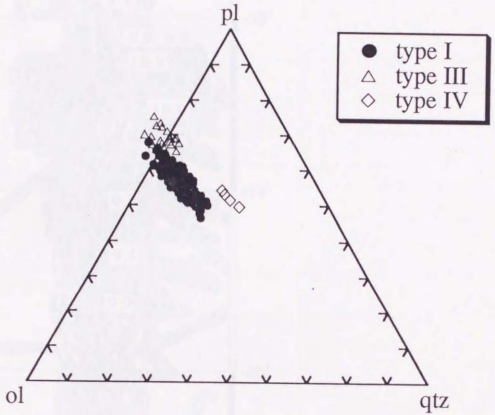

Fig. 27

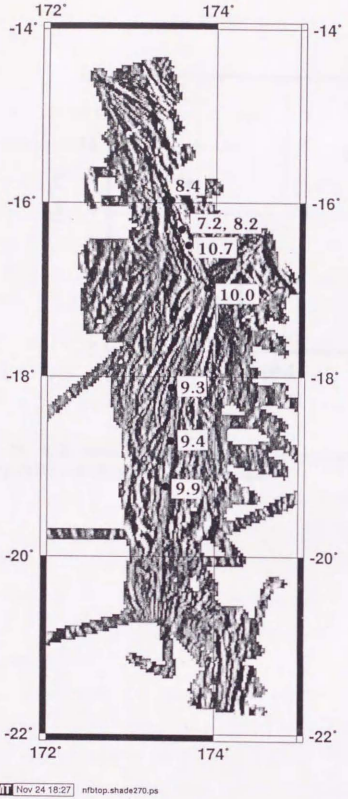

Fig. 28. $^{3}He/^{4}He$ values of the atmospheric ratios (R/R_A) along the axis.

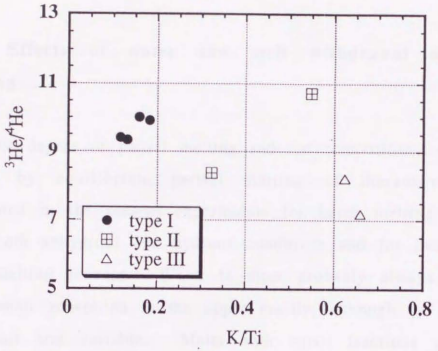

Fig. 29. K/Ti versus $^3He/^4He$ diagram. The geochemically enriched basalts have comparative or slightly lower $^3He/^4He$ ratios.

VI. General discussion

VI-1. Effects of water and melt withdrawal on partial melting

The degree of partial melting and the compositions of melts formed by equilibrium partial melting of lherzolites were determined in the present experiments for batch melting process under both anhydrous and hydrous conditions and for incremental batch melting process. Water is most probably always present during melt generation in the upper mantle, although its amounts are small and variable. Melts with small fractions probably segregate from the host peridotite, and the melting process can be controlled by near fractional melting. However, the effect of small amounts of H_2O (0.1 wt.%~) and that of melt withdrawal in the near fractional melting or incremental batch melting process on partial melting has not ever been estimated quantitatively (Green, 1979; Kushiro, 1990; Kinzler and Grove, 1992a). The comparison of the present experimental results makes it possible to estimate their effects on partial melting.

The degree of partial melting is one of the most principal data in modelling the melt generation in the upper mantle (e.g. Klein and Langmuir, 1987; Mckenzie and Bickle, 1988). The thickness of oceanic crust, for example, directly reflects the volume of melts formed beneath ridges (Mckenzie, 1984; Klein and Langmuir, 1987). From the experimental results given in session II-IV, it is recognized that the presence of water and the melt withdrawal in the incremental batch melting process significantly change the volume of melt compared to that formed by batch melting under

anhydrous conditions (Figs. 12 and 15). The presence of water significantly increases the degree of partial melting; the melt fraction 12-15 % can be produced at 1300°C without volatiles, at 1200°C with the presence of 0.2 wt.% H_2O in the source and also at 1100°C with 0.9 wt.% H_2O in the source at 10 kbar. The additions of 0.1, 0.2 and 0.5 wt.% H_2O increase the melt fraction from 12 % to 19, 22 and 30 % respectively at 10 kbar and 1300°C. On the other hand, the melt withdrawal decreases the degree of partial melting; 17 % of melt fraction is produced by batch melting, whereas only 10 % fraction of melts is formed by incremental batch melting at 15 kbar and 1300°C. Both the effects are significant and cannot be ignored on partial melting processes.

The compositions of melts are also dependent on the presence of water and on the melting process. As shown in the present experimental results, the composition of melt with 0.9 wt.% H_2O formed at 10 kbar and 1300°C is similar to that of anhydrous melt formed at 1350°C (Figs. 11 and 13 and Table 8). Melts formed at about 150°C below the dry solidus temperature are enriched in SiO_2 and depleted in MgO compared to the melts formed by the same degree of partial melting under anhydrous conditions. The compositions of accumulated incremental melts are similar to those of batch melts formed at significantly lower temperatures with the same melt fractions at 15 kbar (Fig. 15 and 16 and Table 11). Those of melts formed by decompressional melting are quite different between both the melting processes as discussed below (Figs. 18-20).

VI-2. Magma generation in the upwelling melting column

When melts are formed by adiabatic decompressional melting of the mantle, the volume and compositions of melts generated in the mantle are completely different depending on whether melts are formed by batch melting or by near fractional melting (incremental batch melting). As was experimentally modelled in session IV where the melt is formed at pressures lower than 22.5 kbar within the one-dimensional upwelling column, the composition of accumulated melts formed by incremental batch melting is similar to a batch melt formed at 15 kbar, whereas that of melt formed by batch melting depends on the depth where the melt segregates (Figs. 18 and 19). The volume of melts generated by the incremental batch melting is smaller by about 20 % than that formed by the batch melting formed in a pressure range from 22.5 to 5 kbar (Fig. 17a).

The theoretical and experimental studies suggested that the small fractions of melt can segregate from the host peridotite (Mckenzie, 1984; Riley and Kohlstedt, 1991). When melts segregate, the residual melt fractions are much smaller than the total degree of partial melting of the host peridotite. However, the compositions of melts and the degrees of partial melting of the peridotite are formed by the equilibrium batch melting at each depth, if equilibrium is attained between the solid and melt at each depth during melt transport to the surface and melts are formed in a steady-state within the one-dimensional melting column where the sum of melt and solid flux is constant at each depth (Koyaguchi, personal communication, 1993). When melts are transported by the porous flows, the rate of chemical equilibration is mainly

controlled by the diffusion in solid (e.g. Iwamori, 1993a). The time scale to reach equilibrium for partial melting is suggested by the high pressure melting experiments, showing that the major element compositions in partial melts did not change significantly after 24 hours at 1300°C where the coexisting minerals were 30-50 μm in diameter (Takahashi and Kushiro, 1983; Hirose and Kushiro, 1993). It suggests that melts can be nearly in equilibrium with the minerals 30-50 μm in diameter after 24 hours. For realistic melting situations that the mantle minerals are about 1 mm in diameter, the equilibration would be attained within 30 years, which is much shorter than the time scale for the melt migration by porous flow which is estimated as 10^5 years (e.g. Iwamori, 1993b; Tanimoto and Stevenson, 1993). The equilibrium is nearly attained in terms of both major element compositions and degrees of partial melting during melt migration by porous flows. Geochemical studies, however, estimate the times for magma ascent between a few decades and thousands of years, suggesting that more rapid melt transport by such as channel flows than porous flows is important (e.g. Gill and Condomines, 1992). When the segregated melts are thus chemically isolated from the residual solid during their migration by channel flows, the process can be treated as near fractional melting (e.g. Spiegelman and Kenyon, 1992; Iwamori, 1993b).

When water is present during partial melting, the differences between both the melting process are much more increased. So far as the melts interact with the surrounding peridotite during melt migration, the presence of water significantly changes the melt composition and degree of partial melting as shown in section III (Figs. 12 and 13). On the other hand, when segregated melts are

chemically isolated from the mantle peridotite and the partial melting processes are controlled by the fractional melting, water has little effect on partial melting. Small amounts of melts are generated at temperatures near the wet solidus which is more than 150°C below the dry solidus at 10 kbar (Green, 1979; session III), but after the elimination of hydrous minerals, melts cannot be formed until the temperature increases above the dry solidus, and water does not influence on partial melting yet. This means that when melts are transported with a negligible reaction with the surrounding peridotite after their formation, water does not increase the volume of melts and probably does not change the compositions of accumulated melts significantly, although the volume and compositions of the hydrous fractional melts have not been determined.

It is important, therefore, to estimate the chemical isolation between melt and solid during melt migration that controls the composition of melts and the degree of partial melting (Spiegelman and Kenyon, 1992; Iwamori, 1993b). The effect of water on partial melting also depends on the chemical isolation. Iwamori (1993b) discussed that more than 80 % melt must be sucked into the chemically isolated channels to explain the trace element compositions in residual clinopyroxenes. The chemical isolation depends on the way of melt transport and the diffusion or dispersion rate of each element. The chemical reaction is progressed for elements with relatively high diffusion rates such as FeO/MgO ratios. It means that the effect of melt withdrawal on partial melting is variable for each element with different diffusivity.

Acknowledgements

Dr. I. Kushiro gave technical support and constructive suggestions throughout the work. Dr. T. Kawamoto is quite helpful to make hydrous melting experiments. Dr. K. Kawamura taught about gel preparation. The author thanks the captain, crew and scientists of the STARMER cruises. Drs. T. Koyaguchi and H. Iwamori gave critical comments about melt generation process. The author thanks Drs. K.T. Johnson, T. Fujii, E. Takahashi, S. Yamashita, K. Ozawa and H. Nagahara for their discussion and comments.

References

Aggrey K.E., Muenow D.W. and Sinton J.M. (1988); Volatile abundances in submarine glasses from the North Fiji and Lau back-arc basins, Geochim. Cosmochim. Acta, 52, 2501-2506.

Ahern J.L. and Turcotte D.L. (1979); Magma generation beneath an ocean ridge, Earth Planet. Sci. Lett., 45, 115-122.

Allan J.F., Batiza R., Perfit M.R., Fornari D.J. and Sack R.O. (1989); Petrology of lavas from the Lamont Seamount Chain and adjacent East Pacific Rise, 10°N, J. Petrol., 30, 1245-1298.

Auzende J.M., Lafoy Y.and Marsset B. (1988); Recent 2 J.M. geodynamic evolution of the north Fiji Basin (southwest Pacific), Geology, 16, 925-929.

Baker M.B., Newman S., Beckett J.R. and Stolper E. (1992); Separating liquid from crystals in high-pressure melting experiments using diamond aggregates, Geo. Soc. Amer., Abstr.

Baker M.B. and Stolper E. (1993); Determining the composition of high-pressure mantle melts using diamond aggregates, Geochim. Cosmochim. Acta, submitted.

Bryan W.B. and J.G. Moore J.G. (1977); Compositional variations of young basalts in the mid-Atrantic ridge rift valley near lat 36°49'N, Geol. Soc. Amer. Bull. 88, 556-570.

Danyushevsky L.V., Falloon T.J., Sobolev A.V., Crawford A.J., Carrol M. and Price R.C. (1993); The H_2O content of basalt glasses from southwest Pacific back-arc basin, Earth Planet. Sci. Lett., 117, 347-362.

Delaney J.R., Muenow D.W. and Graham D.G. (1978); Abundance and distribution of water, carbon and sulfer in the glassy rims of submarine pillow basalts, Geochim. Cosmochim. Acta, 581-594.

Eissen J.P., Lefevre C., Maillet P., Morvan G. and Nohara M. (1991); Petrology and geochemistry of the central North Fiji Basin spreading centre (Southwest Pacific) between 16°S and 22°S, Marine Geology, 98, 201-239.

Eissen J.P., Nohara M., Cotten J. amd Hirose K. (1993); The North Fiji Basin basalts and their magma sources: part I. trace and rare earth elements constraints, Marine Geology, in press.

Falloon T.J. and Green D.H. (1987); Anhydrous partial melting of MORB pyrolite and other peridotite compositions at 10 kbar: Implications for the origin of primitive MORB glasses, Mineral. Petrol., 37, 181-219.

Falloon T.J., Green D.H., Hatton C.J. and Harris K.L. (1988); Anhydrous partial melting of a fertile and depleted peridotite from 2 to 30 kb and application to basalt petrogenesis, J. Petrol. 29, 1257-1282.

Falloon T.J. , Malahoff A., Zonenshain L.P. and Bogdanov Y. (1991); Petrology and geochemistry of back-arc basin basalts from Lau Basin spreading ridges at 15, 18 and 19°S, submitted to Mineral. Petrol.

Farley K.A., Natland J. and Craig H. (1992); Binary mixing of enriched and undegassed (primitive?) mantle components (He, Sr, Nd, Pb) in Samoan lavas, Earth Planet. Sci. Lett., 111, 183-199.

Fujii T. (1989); Genesis of mid-ocean ridge basalts, in: Magmatism in the Ocean Basins, A.D. Saunders and M.J. Norry, ed., pp. 137-146, Geol. Soc. Spec. Publ.

Fujii T. and Bougault H. (1983); Melting relations of a magnesian abyssal tholeiite and the origin of MORBs, Earth Planet. Sci. Lett., 62, 283-295.

Fujii T. and Scarfe C.M. (1985); Composition of liquid coexisting with spinel lherzolite at 10 kbar and the genesis of MORBs, Contrib. Mineral. Petrol. 90, 18-28.

Garcia M.O., Lin N.W.K. and Muenow D.W. (1979); Volatiles in submarine volcanic rocks from the Mariana island arc and trough, Geochim. Cosmochim. Acta, 43, 305-312.

Gill J. and Condomines M. (1992); Short lived radioactivity and magma genesis, Science, 257, 1368-1376.

Green D.H. (1973); Experimental melting studies on a model upper mantle composition of high pressure under water-saturated and water-undersaturated conditions, Earth Planet. Sci. Lett., 19, 37-45.

Hirose K. and Kushiro I. (1992); Partial melting of dry peridotites at high pressures: Determination of compositions of melts segregated from peridotite using aggregates of diamond, EOS, 73, 615 (Abstr).

Hirose K. and Kushiro I. (1993); Partial melting of dry peridotites at high pressures: Determination of compositions of melts segregated from peridotite using aggregates of diamond, Earth Planet. Sci. Lett., 114, 477-489.

Hirose K., Nohara M., Hiyagon H., Tanahashi M. and Eissen J.P. (1993); Petrology of the central ridge in the North Fiji Basin, Earth Planet. Sci. Lett., in revision.

Hiyagon H., Ojima M., Marty B., Zashu S. and Sakai H. (1992); Noble gases in submarine glasses from mid-oceanic ridges and Loihi seamount: Constraints on the early history of the earth, Geochim. Cosmochim. Acta, 56, 1301-1316.

Hawkins J.W. and Melchior J.T. (1985); Petrology of Mariana Trough and Lau Basin basalts, J. Geophys. Res., 90, 11431-11468.

Hawkins J.W., Lonsdale P.F., Macdougall J.D. and Volpe A.M. (1990); Petrology of the axial ridge of the Mariana Trough backarc spreading center, Earth Planet. Sci. Lett., 100, 226-250.

Irvine T.N. and Baragar W.R. (1971); A guide to the chemical classification of the common volcanic rocks, Can. J. Earth. Sci. 8, 523-548.

Iwamori H. (1993a); Dynamic disequilibrium melting model with porous flow and diffusion-controlled chemical equilibration, Earth Planet. Sci. Lett., 114, 301-313.

Iwamori H. (1993b); A model for disequilibrium mantle melting incorporating melt transport by porous and channel flows, Nature, in press.

Jambon A. and Zimmermann J.L. (1990); Water in oceanic basalts: evidence for dehydration of recycled crust, Earth Planet. Sci. Lett., 101, 323-331.

Johnson K.T.M. and Sinton J.M. (1990); Petrology, tectonic setting, and the formation of back-arc basin basalts in the North Fiji Basin, Geol. Jb, D92, 517-545.

Johnson K.T., Dick H.J. and Shimizu N. (1990); Melting in the oceanic upper mantle: an ion microprobe study of diopsides in abyssal peridotites, J. Geophy. Res. 95, 2661-2678.

Johnson K.T. and Kushiro I. (1992); Segregation of high pressure partial melts from peridotite using aggregates of diamond: a new experimental approach, Geophy. Res. Lett., 19, 1703-1706.

Jaques, A.L. and Green D.H. (1980); Anhydrous melting of peridotite at 0-15 kbar pressure and the genesis of tholeiitic basalts, Contrib. Mineral. Petrol., 73, 287-310.

Kawamoto T. and Hirose K. (1993); Au-Pd sample containers for melting experiments on iron and water bearing systems, Europ. J. Mineral., submitted.

Kinzler R.J. and T.L. Grove T.L. (1992a); Primary magmas of mid-ocean ridge basalts 1. Experiments and methods, J. Geophy. Res., 97, 6885-6906.

Kinzler R.J. and T.L. Grove T.L. (1992b); Primary magmas of mid-ocean ridge basalts 2. Applications, J. Geophy. Res., 97, 6907-6926.

Kinzler R.J. and T.L. Grove T.L. (1993); Corrections and further discussion of the primary magmas of mid-ocean ridge basalts, 1 and 2, J. Geophy. Res., submitted.

Klein E.M. and Langmuir C.H. (1987); Global correlations of ocean ridge basalt chemistry with axial depth and crustal thickness, J. Geophy. Res. 92, 8089-8115.

Kuno H. (1960); High-alumina basalt, J. Petrol. 1, 121-145.

Kushiro I. (1976); A new furnace assembly with a small temperature gradient in solid-media, high-pressure apparatus, Carnegie Inst. of Washington Year Book 75, 832-833.

Kushiro I. (1968); Compositions of magmas formed by partial zone melting of the earth's upper mantle, J. Geophy. Res. 73, 619-634.

Kushiro I. (1990); Partial melting of mantle wedge and evolution of island arc crust, J. Geophy. Res., 95, 15929-15939.

Kushiro I. (1993); Partial melting of a fertile mantle peridotite at high pressures: An experimental study using aggregates of diamond, J. Geophy. Res., submitted.

Kushiro I. and Hirose K. (1992); Experimental determination of composition of melt formed by equilibrium partial melting of peridotite at high pressures using aggregates of diamond grains, Proc. Japan Acad. 68, 63-68.

Kushiro I. and Thompson R.N. (1972); Origin of some abyssal tholeiites from the Mid-Atlantic ridge, Carnegie Inst. of Washington Year Book 71, 403-406.

Kushiro I., Y. Syono Y. and S. Akimoto S. (1968); Melting of a peridotite nodule at high pressures and high water pressures, J. Geophy. Res. 73, 6023-6029.

Koyaguchi T. (1989); Chemical gradient at diffusive interfaces in magma chambers, Contrib. Mineral. Petrol. 103, 143-152.

Langmuir C.H., Klein E. M. and Plank T. (1992); Petrological systematics of mid-ocean ridge basalts: Constraints on melt generation beneath ocean ridges, in Mantle flow and melt generation at mid-ocean ridges, Geophys. Monogr. 71, edited by J.P. Morgan, D.K. Blackman and J.M. Sinton, AGU, Washington, D.C..

LaTraille S.L. and Hussong D.M. (1980); Crustal structure across the Mariana island arc, in The tectonic and geological evolution of southeast Asian seas and islands, Part 1, Geophys. Monogr. 23, edited by D.E. Hayes, pp. 209-222, AGU, Washington, D.C..

Leg 135 Scientific Party (1992); Evolution of backarc basins: ODP Leg 135, Lau Basin, Eos trans., 73, 241-247.

Lewis B.T.R. and Snydsman W.E. (1982); Fine structure of the lower oceanic crust on the Cocos plate, Tectonophysics, 55, 87-105.

Maaløe S. and K. Aoki K. (1977); The major element composition of the upper mantle estimated from the compositions of lherzolites, Contrib. Mineral. Petrol. 63, 161-173.

Malahoff A., Hammond S.R., Naughton J.J., Keeling D.L. and Richmond R.N. (1982); Geophysical evidence for post-Miocene rotation of the island of Viti Levu, Fiji, and its relationship to the tectonic development of the North Fiji Basin, Earth Planet. Sci. Lett., 57, 398-414.

Mckenzie D. (1984); The generation and compaction of partially molten rock, J. Petrol., 25, 713-765.

Mckenzie D. (1985); ^{230}Th-^{238}U disequilibrium and the melting processes beneath ridge axes, Earth Planet. Sci. Lett. 72, 149-157.

Mckenzie D. and M.J. Bickle M.J. (1988); The volume and composition of melt generated by extension of lithosphere, J. Petrol, 29, 625-679.

Michael P.J. and Chase R.L. (1987); The influence of primary magma composition, H_2O and pressure on mid-ocean ridge basalt differentiation, Contrib. Mine. Petrol., 96, 245-263.

Muenow D.W., Garcia M.O., Aggrey K.E., Bednarz U. and Schminke H.U. (1990); Volatiles in submarine glasses as a discriminant of tectonoc origin: application to the Troodos ophiolite, Nature, 343, 159-161.

Muenow D.W., Niu N.W.K., Garcia M.O. and Saunders A.D. (1980); Volatiles in submarine volcanic rocks from the spreading axis of the East Scotia Sea back-arc basin, Earth Planet. Sci. Lett., 47, 272-278.

Mysen B. and Kushiro I. (1977); Compositional variations of coexisting phases with degree of melting of peridotite in the upper mantle, Am. Mineral., 62, 843-865.

Niu Y. and Batiza R. (1991); An empirical method for calculating melt compositions produced beneath mid-ocean ridges: Application for axis and off-axis (seamounts) melting, J. Geophys. Res., 96, 21753-21777.

Nixon P.H. and Boyd F.R. (1973); Petrogenesis of the granular and sheared ultrabasic nodule suite in kimberlites, in Lesotho Kimberlites, P.H. Nixon ed., Lesotho national development Co., Lesotho, pp. 48-56.

Nohara M., Hirose K., Eissen J.P., Urabe T. and Joshima M. (1993); Isotope and trace element geochemistry of the North Fiji Basin basalts: part II. Implications for the evolution of magma sources and mantle heterogeneity, Marine Geology, in press.

Price R.C., Johnson L.E. and Crawford A.J. (1990); Basalts of the North Fiji Basin: the generation of back arc basin basalts by mixing of depleted and enriched mantle sources, Contrib. Mine. Petrol., 105, 106-121.

Presnall D.C. (1969); The geometrical analyses of partial fusion, Am. J. Sci., 267, 1178-1194.

Presnall D.C. and J.D. Hoover (1987); High pressure phase equilibrium constraints on the origin of mid-ocean ridge basalts, in Magmatic processes: Physicochemical principles, Special publication no.1, pp. 75-89, edited B.O. Mysen, the geological society.

Riley Jr. G.N. and Kohlstedt D.L. (1991); Kinetics of melt migration in upper mantle-type rocks, Earth Planet. Sci. Lett., 105, 500-521.

Rushmer T. (1991); Partial melting of two amplibolites: contrasting experimental results under fluid absent conditions, Contrib. Mineral. Petrol., 107, 41-59.

Searle R.C. (1976); Lithosphere structure of the Azores plateau from Rayleigh-wave dispersion, Geophys. J. R. Astron. Soc., 44, 537-546.

Sakuyama M. (1979); Lateral variations of H2O contents in Quaternary magmas of northeastern Japan, Earth Planet. Sci. Lett., 43, 103-111.

Schilling J.G., Zajac M., Evans R., Johnston T., White W., Devine J.D. and Kingsley R. (1983); Petrologic and geochemical variations along Mid-Atlantic Ridge from 29°N to 73°N, Am. J. Sci., 283, 510-586.

Sinton J.M. and Fryer P. (1987); Mariana Trough lavas from 18°N: implications for the origin of back arc basin basalts, J. Geophys. Res., 92, 12782-12802.

Sinton J.M., Price R.C., Johnson K.T., Staudigel H. and Zindler A. (1988); Petrology and geochemistry of submarine lavas from the Lau and North Fiji back-arc basins, in: Basin formation ridge crest processes, and metallogenesis in the North Fiji Basin, Circum-Pacific Council for energy and mineral resources, L.W. Kroenke and J.V. Eade, ed., pp. 1-23.

Smith D., Griffin W.L. and Ryan C.G. (1993); Compositional evolution of high temperature sheared lherzolite PHN 1611, Geochim. Cosmochim. Acta, 57, 605-613.

Sobolev A.V. and Shimizu N. (1993); Ultra-depleted primary melt included in an olivine from the Mid-Atlantic Ridge, Nature, 363, 151-154.

Spiegelman M. and Kenyon P. (1992); The requirements for chemical disequilibrium during magma migration, Earth Planet. Sci. Lett., 109, 611-620.

Stolper E. (1980); A phase diagram for mid-ocean ridge basalts: preliminary results and implications for petrogenesis, Contrib. Mineral. Petrol. 74, 13-27.

Sun S. and McDonough W.F. (1989); Chemical and isotopic systematics of oceanic basalts: implications for mantle composition and processes, Magmatism in the Ocean Basins, A.D. Saunders and M.J. Norry, ed., pp. 313-345.

Sweeney R.J., Falloon T.J., Green D.H. and Tatsumi Y. (1991); The mantle origins of Karoo picrites, Earth Planet. Sci. Lett., 107, 256-271.

Takahashi E. and Kushiro I. (1983); Melting of a dry peridotite at high pressures and basalt magma genesis, Amer. Mineral. 68, 859-879.

Takahashi E. (1986); Melting of a dry peridotite KLB-1 up to 14 GPa: implications on the origin of peridotitic upper mantle, J. Geophy. Res., 91, 9367-9382.

Takahashi E. (1989); Partial melting experiments of lower crustal materials II, Volcanol. Soc. Japan, Fall meeting, B69, Abstr. (in Japanese).

Takahashi E., Shimazaki T., Tsuzaki Y. and Yoshida H. (1992); Melting study of a peridotite KLB-1 to 6.5 GPa and origin of basaltic magmas, Phil. Trans. Royal Soc. London, in press.

Tamaki K., Suehiro K., Allan J., Ingle J.C. Jr. and Pisciotto K.A. (1992); Tectonic sysnthesis and implications of Japan sea ODP drilling, Proced. ODP Program, Scientific Results, 127/128, 1333-1348.

Tanahashi M., Kisimoto K., Joshima M., Lafoy Y., Honza E. and Auzende J.M. (1991); Geological structure of the central spreading system, North Fiji Basin, Marine Geology, 98, 187-200.

Tanimoto T. and Stevenson D.J. (1993); Seismic constraints on partial melts under ridge axes, submitted to J. Geophy. Res..

Walker D., Shibata T. and DeLong S.E. (1979); Abyssal tholeiites from the Oceanographer fracture zone II, phase equilibria and mixing, Contrib. Mineral. Petrol. 70, 111-125.

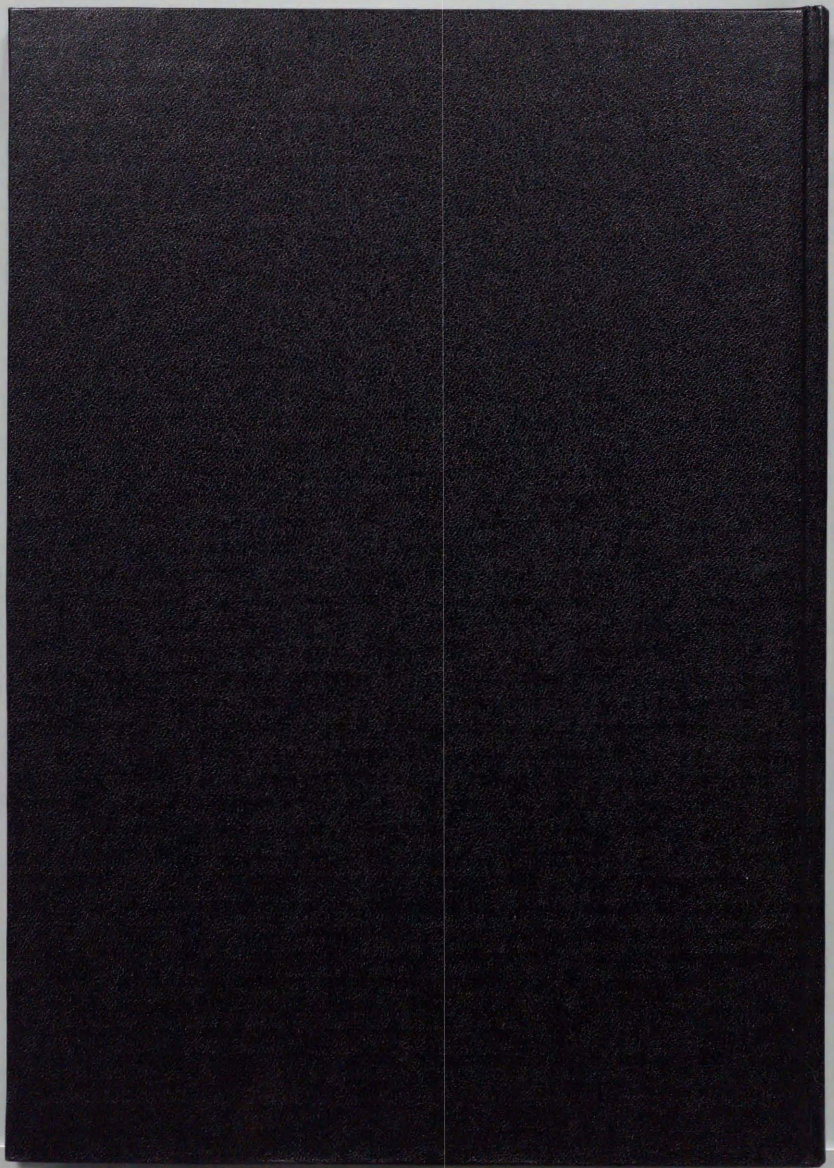

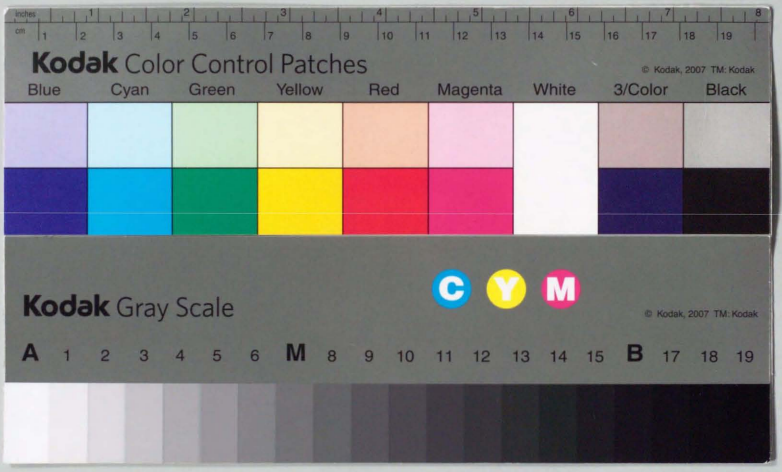
inches
cm
Kodak Color Control Patches
© Kodak, 2007 TM: Kodak
Blue
Cyan
Green
Yellow
Red
Magenta
White
3/Color
Black
Kodak Gray Scale
C
Y
M
© Kodak, 2007 TM: Kodak
A 1 2 3 4 5 6 M 8 9 10 11 12 13 14 15 B 17 18 19